https://doi.org/10.5194/egusphere-2025-616
Preprint. Discussion started: 14 February 2025

Seasonality of meridional overturning in the subpolar North Atlantic: implications for relying on the streamfunction maximum as a metric of AMOC slowdown

Alan D. Fox[1], Neil J. Fraser[1], and Stuart A. Cunningham[1]

[1]Scottish Association for Marine Science, Oban, UK

Correspondence: Alan D. Fox (alan.fox@sams.ac.uk)

Abstract.

Atlantic meridional overturning circulation has a notable seasonal component. This influences the jet stream and the location, frequency and intensity of extreme weather events. Understanding this seasonality is important for mitigating the impacts of AMOC changes on European weather and climate. Here we place meridional overturning and fluxes in a coherent framework. This framework highlights the integral relationship between meridional overturning circulation and property transports, both being functions purely of the overturning streamfunction Ψ. Using this framework we examine the seasonality observed in overturning and density, temperature and freshwater fluxes at the OSNAP line in the subpolar North Atlantic. We find the seasonal cycle of the MOC metric (the standard measure of overturning defined as the maximum of the overturning streamfunction) to be dominated by Ekman transports and the large-scale seasonal cycle of surface density; heat flux to be dominated by barotropic velocity variability; the seasonal cycle of freshwater flux by a combination of barotropic velocities and the salinity in the western boundary current; and density flux to reflect a broad range of characteristics and processes. We show that the MOC metric is a poor predictor, on seasonal time-scales, of either density fluxes or the more societally relevant ocean heat and freshwater transports. This is due to each of these metrics responding to different physical processes. The MOC metric, on seasonal timescales at least, has very high sensitivity to near-surface physical characteristics in a limited geographical area. These characteristics are not necessarily reflective of the fundamental processes driving overturning. Therefore, we suggest caution in the use of the standard MOC metric when studying overturning, and the routine use of the density flux as a valuable additional overturning metric.

1 Introduction

Atlantic meridional overturning circulation (AMOC) has a notable seasonal component. This influences the jet stream and the location, frequency and intensity of extreme weather events. Understanding this seasonality is important for mitigating the impacts of AMOC changes on European weather and climate. Driven by innovation in ocean observation, theory and modelling our understanding of subpolar North Atlantic meridional overturning has advanced rapidly in recent years. Basin-wide observational arrays, particularly OSNAP (Overturning in the Subpolar North Atlantic Program, Lozier et al., 2019), now allow robust estimation of the seasonal cycle in the strength of subpolar overturning and associated heat and freshwater

https://doi.org/10.5194/egusphere-2025-616
Preprint. Discussion started: 14 February 2025

transports (Gary et al., 2018; Fu et al., 2023; Fraser et al., 2024; Mercier et al., 2024). Theoretical models of overturning (see Johnson et al., 2019, for a review of the state of the art) help us understand the interplay between surface buoyancy and wind forcing, and provide new paradigms for deep water formation. Meanwhile global-scale high resolution ocean models (e.g. Hirschi et al., 2020; Biastoch et al., 2021), and state estimates (Forget et al., 2015) allow us to make detailed examination of dynamics and mechanisms.

While the driving processes of Atlantic meridional overturning circulation (AMOC) – winds, surface fluxes and freshwater input – have marked seasonal cycles at subpolar latitudes, it remains unclear how, or if, these seasonal cycles are expressed in the observations of AMOC and related transports on basin-wide sections such as OSNAP. Observational and modelling studies of subpolar North Atlantic meridional overturning consistently return estimates of the seasonal cycle of overturning, as measured by the maximum of the overturning streamfunction (MOC_σ), with amplitude of about 4 Sv with a late spring maximum and autumn or winter minimum (Lozier et al., 2019; Fu et al., 2023; Wang et al., 2021; Tooth et al., 2023; Mercier et al., 2024). These studies find overturning seasonality, as for the mean subpolar overturning (Lozier et al., 2019; Petit et al., 2020), to be dominated by water transformation north of a line linking Greenland and Scotland rather than in the Labrador Sea.

Analyses of OSNAP observations (Fu et al., 2023) show the subpolar AMOC seasonal cycle to be dominated by seasonality in the Irminger Basin, particularly the East Greenland Current, modified by Ekman transport driven by seasonality in the zonal winds. The East Greenland Current seasonality is ascribed to a lagged signal of watermass transformation in the Irminger Basin. Examination of an ocean reanalysis (Wang et al., 2021) and detailed observations (Le Bras et al., 2020) suggest the seasonal cycle of overturning closely follows *density variability* in the western boundary current. However, other observations show (Mercier et al., 2024; Le Bras et al., 2018) the *seasonal transport variability* in the western boundary current also to be an important contributor to AMOC seasonal cycle. The combined effect of density and transport seasonality is explored in results from a high resolution ocean hindcast model (Tooth et al., 2023), with innovative use of Lagrangian tracking used to attribute transport variability to variability of particle transit times round the northern subpolar Gyre. Seasonality in zonal winds is a common theme dominating MOC seasonality at lower latitudes (Yang, 2015; Zhao and Johns, 2014), with geostrophic transport at the boundaries and in the interior, perhaps in turn driven by wind-stress curl or a lagged response to deep-water formation, controlling the seasonal cycle at higher latitudes (Chidichimo et al., 2010; Zhao and Johns, 2014; Gary et al., 2018; Tooth et al., 2023; Mercier et al., 2024).

The maximum of the overturning streamfunction, integrated across the width of the basin and calculated variously in density (MOC_σ) or depth (MOC_z) space, has become synonymous with the strength of the meridional overturning circulation on a given transatlantic section. Indeed we will use it in this sense in the current work. In a wider, ocean conveyor-belt, sense, in the North Atlantic and Arctic basins the meridional overturning circulation is fundamentally a water transformation process – lighter surface waters flowing north, being transformed to denser waters, sinking, mixing and flowing south. Observational arrays such as OSNAP (Lozier et al., 2019) and RAPID (Cunningham et al., 2007; Kanzow et al., 2007) attempt to quantify these transformation processes by monitoring the north-south exchanges along basin-wide sections. On shorter, seasonal and inter-annual, timescales it is clear that the 'overturning' signal observed at these arrays does not purely represent this wider, large-scale, overturning. Adiabatic, 'sloshing' motions (Han, 2023a, b; Fraser et al., 2025) driven by Ekman transport and

https://doi.org/10.5194/egusphere-2025-616
Preprint. Discussion started: 14 February 2025

wind-stress curl (Fraser et al., 2024) dominate observed MOC_σ on shorter timescales. Seasonal cycles of surface mixed layer warming and cooling, deepening and shallowing will also be expressed in the seasonal cycle of the overturning streamfunction, even where these changes are not ultimately subducted into the ocean interior and the overturning circulation (Tooth et al., 2023).

Here we attempt to disentangle the various processes expressed in the MOC_σ and overturning streamfunction at the OSNAP line. To do this we adopt and extend the formalism proposed by Mercier et al. (2024). We use these methods to examine the seasonal cycle in the full density-space overturning streamfunction, rather than focussing exclusively on MOC_σ (the maximum of the streamfunction). We advocate for the routine use of the northward density flux (e.g. Fraser and Cunningham, 2021), which we show can be calculated as the area under the overturning streamfunction curve, as an additional metric alongside the MOC to give a more complete understanding of overturning. This density flux is a somewhat neglected part of the watermass transformation theory (Tziperman, 1986; Speer and Tziperman, 1992; Nurser et al., 1999) which fundamentally underpins the concept of overturning, and has close parallels with both heat and freshwater transports. Using this framework, beginning with analysis of the output of a high-resolution model hindcast, we aim to produce a more comprehensive and integrated description of the seasonal cycle of overturning observed on the OSNAP line, encompassing MOC_σ, density flux, and heat and freshwater transports. We consider how each of these important overturning metrics responds differently to the underlying mechanisms driving the overturning. The model-derived hypotheses obtained are then tested against the seasonal cycle in the OSNAP observational timeseries, possible implications for AMOC and climate studies examining variability on longer timescales are discussed.

2 Methods

2.1 Data

We conduct the model analysis using output from the 1/20° VIKING20X JRA55-short model hindcast of the North Atlantic (Biastoch et al., 2021; Getzlaff and Schwarzkopf, 2024). Model results presented in the main text are based on the final 20 years of this run, 2000 to 2019 (Supplementary Information contains results based on the 2014 to 2019 period to more closely match the observational period).

For the observational analysis we use the OSNAP 6-year gridded dataset and time series (Fu et al., 2023) and ERA5 surface wind stress (Hersbach et al., 2020, 2023). For parts of the analysis we divide the OSNAP line at Greenland into OSNAP West ($\mathrm{OSNAP_W}$) and OSNAP East ($\mathrm{OSNAP_E}$). ERA5 wind stresses are interpolated onto the OSNAP gridded observation points and used to calculate Ekman transports across the OSNAP section.

2.2 Theoretical framework

The zonally integrated overturning streamfunction in density space, $\Psi_\sigma(\sigma, t)$, can be written:

https://doi.org/10.5194/egusphere-2025-616
Preprint. Discussion started: 14 February 2025

$$\Psi_\sigma(\sigma,t) = \int_w^e \int_{\sigma_{\min}}^{\sigma} v \frac{\partial z}{\partial \sigma} \, d\sigma \, dx \tag{1}$$

where x is the along-section coordinate from minimum ($x = w$) to maximum ($x = e$), z is the vertical coordinate (positive upwards), v is the velocity normal to the section. Ψ has units of $\mathrm{m^3\,s^{-1}}$, or more commonly Sv (Sverdrup, where $1\,\mathrm{Sv} = 1 \times 10^6\,\mathrm{m^3\,s^{-1}}$). Note that we integrate from low to high density. The direction of integration makes no difference when the total volume transport through the section is zero. On the OSNAP line there is generally a small net southward flow, integrating from high to low density then leads to small offsets in overturning and transports. Importantly for the work presented here the direction of integration has very little impact on the anomalies (zero impact for the observations where net transports are fixed).

We then define the meridional overturning, $\mathrm{MOC}_\sigma(t)$, as the maximum of Ψ_σ for all σ, and $\sigma_{\mathrm{MOC}}(t)$ as the density at which this maximum occurs:

$$\mathrm{MOC}_\sigma(t) = \max_\sigma \left[\Psi_\sigma(\sigma,t)\right] \tag{2}$$

$$\sigma_{\mathrm{MOC}}(t) = \arg\max_\sigma \left[\Psi_\sigma(\sigma,t)\right] \tag{3}$$

The zonally and depth integrated meridional density flux ($\mathcal{D}$) can be written:

$$\mathcal{D} = \int_w^e \int_{-H}^{\eta} v\sigma \, dz \, dx \tag{4}$$

where H is the water depth and η the surface elevation. We follow convention in referring to this as 'density flux' while the units of $\mathrm{kg\,s^{-1}}$ suggest 'mass flux'. It is not a true mass flux as steric height changes are ignored in both model (via the Boussinesq approximation) and observational (surface defined as $z = 0$) calculations. The term 'density flux' captures the process intuitively – with lighter water flowing northwards and denser water returning southward being characterised as a southward (or negative northward) density flux.

Rearranging Eq. 4, we can write this density flux as a function of the overturning streamfunction. Changing vertical coordinate from z to σ and integrating by parts, Eq. 4 becomes:

$$\mathcal{D} = \sigma_{max} \int_w^e \int_{\sigma_{\min}}^{\sigma_{\max}} v \frac{\partial z}{\partial \sigma} d\sigma \, dx \; - \int_{\sigma_{\min}}^{\sigma_{\max}} \Psi_\sigma \, d\sigma \tag{5}$$

The first term on the RHS of Eq. 5 is just a multiple of the net volume transport through the section. For the trans-ocean sections and transport anomalies considered here this net volume transport is small and the first term can be ignored. So we have:

$$\mathcal{D} = - \int_{\sigma_{\min}}^{\sigma_{\max}} \Psi_\sigma \, d\sigma \tag{6}$$

https://doi.org/10.5194/egusphere-2025-616
Preprint. Discussion started: 14 February 2025

We have calculated the density flux using both Eqs. 4 and 6 and it makes no significant difference to our results.

A quick note on terminology. Throughout we use the terms 'overturning streamfunction' to refer to $\Psi(\sigma,t)$ and 'meridional overturning' or 'MOC' to refer to the maximum of Ψ in density space.

Note that the density-space equations have analogues in both temperature and salinity space, for the sake of brevity and clarity we will discuss temperature and salinity space results only briefly, and purely in the context of heat and freshwater transports, but the relevant equations are given here. In temperature, θ, space we have the overturning streamfunction (Ψ_θ), meridional overturning (MOC_θ), and meridional heat transport ($\mathcal{H}$). We choose to integrate downwards in temperature space, from high to low, which reverses the sign in the heat transport equation below.

$$\Psi_\theta(\theta,t) = \int_w^e \int_\theta^{\theta_{\max}} v \frac{\partial z}{\partial \theta}\, d\theta\, dx \tag{7}$$

$$\mathrm{MOC}_\theta(t) = \max_\theta [\Psi_\theta(\theta,t)] \tag{8}$$

$$\theta_{\mathrm{MOC}}(t) = \arg\max_\theta [\Psi_\theta(\theta,t)] \tag{9}$$

$$\mathcal{H} = \rho \mathrm{C_p} \int_{\theta_{\min}}^{\theta_{\max}} \Psi_\theta\, d\theta \tag{10}$$

where ρ is potential density and $\mathrm{C_p}$ the specific heat capacity of sea water. Finally, in salinity, S, space we have the overturning streamfunction (Ψ_S), meridional overturning (MOC_S), and northward meridional freshwater transport ($\mathcal{F}$). In salinity space the sign of the overturning streamfunction is usually reversed, with net freshwater input in the north opposing the overturning. So we define $\mathrm{MOC}_S(t)$ as the minimum of Ψ_S rather than the maximum. We also convert northward salinity transports to freshwater transports using a section mean reference salinity, $\overline{S}$. Hence,

$$\Psi_S(S,t) = \int_w^e \int_{S_{\min}}^{S} v \frac{\partial z}{\partial S}\, dS\, dx \tag{11}$$

$$\mathrm{MOC}_S(t) = \min_S [\Psi_S(S,t)] \tag{12}$$

$$S_{\mathrm{MOC}}(t) = \arg\min_S [\Psi_S(S,t)] \tag{13}$$

$$\mathcal{F} = \frac{1}{\overline{S}} \int_{S_{\min}}^{S_{\max}} \Psi_S\, dS \tag{14}$$

These relationships are displayed graphically for the mean overturning streamfuctions in Figs. 1 and 2. Using this framework it becomes clear that in each space MOC and property transports are intimately linked, one being the maximum and the other the integral of Ψ. We can imagine scenarios in which variability of the two could be either strongly correlated (e.g. a simple

https://doi.org/10.5194/egusphere-2025-616
Preprint. Discussion started: 14 February 2025

amplification of the flow), or entirely decoupled (e.g. surface warming of upper limb water driving increased northward heat transport but having no effect on MOC).

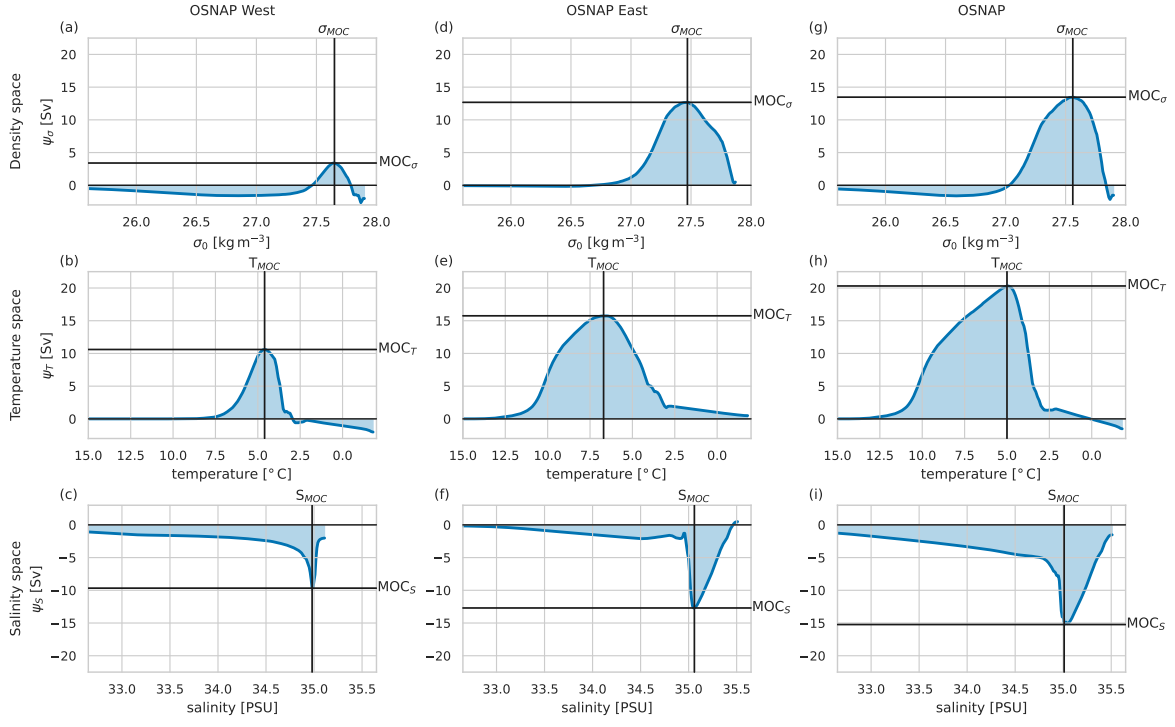

Figure 1. Mean overturning streamfunctions from 20-years of Viking20x model. The left-hand column (panels a-c) shows $\mathrm{OSNAP_W}$, the centre column (d-f) $\mathrm{OSNAP_E}$ and the right-hand column (g-i) the full OSNAP transect. In each case the top row (a,d,g) is the overturning streamfunction in density space, the middle row (b,e,h) in temperature space, and the bottom row (c,f,i) salinity space. The maximum overturning (negative in salinity space) is highlighted in each case, labelled MOC, along with the property value at which it occurs (σ_{MOC} for density, T_{MOC} for temperature, and S_{MOC} for salinity). The shaded integrated areas under the curve are proportional to the southward density flux (top row), the northward heat flux (middle row) and the northward freshwater flux (bottom row, negative shows net freshwater flux is southward). The plots are scaled such that unit area in each case very approximately corresponds to the same density flux – MOC_σ and the southward density flux are a combination of northward heat flux opposed by southward freshwater flux.

2.3 Streamfunction decomposition

We decompose the streamfunction variability into parts associated with velocity variability, density structure variability and co-variation of density and velocity fields Mercier et al. (2024).

Rewriting Eq. 1 we have

https://doi.org/10.5194/egusphere-2025-616
Preprint. Discussion started: 14 February 2025

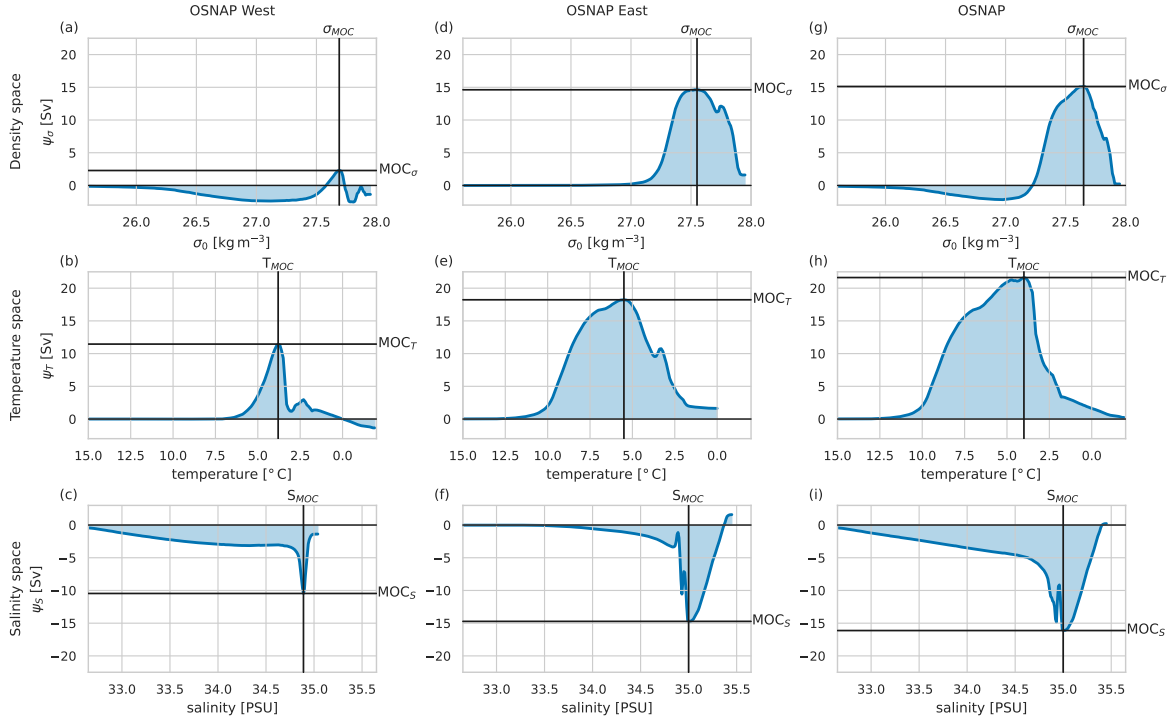

Figure 2. As for Fig. 1 but for the overturning from the 6-year OSNAP observational timeseries.

$$\Psi_\sigma(\sigma,t) = \int_w^e \int_{z_\sigma(\sigma)}^{z_\sigma(0)} v(x,z,t)\,dz\,dx \tag{15}$$

where $z_\sigma(\sigma) = z_\sigma(\sigma,z,t)$ is the depth of the σ isopycnal at position x and time t.

We can decompose the velocity field into time-mean, $\overline{v}$, and variable, v', parts and the isopycnal depths into a time-mean part, $\overline{z}_\sigma$, and a deviation from the time-mean z'_σ

$$v = \overline{v} + v' \tag{16}$$

$$z_\sigma = \overline{z}_\sigma + z'_\sigma. \tag{17}$$

We can then rewrite Eq. 15

https://doi.org/10.5194/egusphere-2025-616
Preprint. Discussion started: 14 February 2025

$$\Psi_\sigma(\sigma,t) = \int_w^e \int_{\overline{z}_\sigma(\sigma)+z'_\sigma(\sigma)}^{z_\sigma(0)} \overline{v}(x,z)\,dz\,dx + \int_w^e \int_{\overline{z}_\sigma(\sigma)+z'_\sigma(\sigma)}^{z_\sigma(0)} v'(x,z,t)\,dz\,dx \tag{18}$$

$$\begin{aligned} &= \int_w^e \int_{\overline{z}_\sigma(\sigma)}^{z_\sigma(0)} \overline{v}\,dz\,dx + \int_w^e \int_{\overline{z}_\sigma(\sigma)+z'_\sigma(\sigma)}^{\overline{z}_\sigma(\sigma)} \overline{v}\,dz\,dx \\ &\quad + \int_w^e \int_{\overline{z}_\sigma(\sigma)}^{z_\sigma(0)} v'\,dz\,dx + \int_w^e \int_{\overline{z}_\sigma(\sigma)+z'_\sigma(\sigma)}^{\overline{z}_\sigma(\sigma)} v'\,dz\,dx \end{aligned} \tag{19}$$

where the first and third terms on the RHS are integrals between the mean depth of the σ isopycnal and the surface, and the second and fourth terms integrate between the instantaneous and mean depths of the σ isopycnal. We write this more concisely as

$$\Psi_\sigma(\sigma,t) = \Psi_{\overline{\sigma}\,\overline{v}}(\sigma) + \Psi_{\sigma'\,\overline{v}}(\sigma,t) + \Psi_{\overline{\sigma}\,v'}(\sigma,t) + \Psi_{\sigma'\,v'}(\sigma,t) \tag{20}$$

Removing the long-term mean ($\overline{\Psi_\sigma}$) from all terms and taking monthly means to examine the seasonal cycle leaves:

$$\Psi'_\sigma(\sigma,m) = \Psi'_{\sigma'\,\overline{v}}(\sigma,m) + \Psi'_{\overline{\sigma}\,v'}(\sigma,m) + \Psi'_{\sigma'\,v'}(\sigma,m) \tag{21}$$

where m now indicates these are mean monthly anomalies from the long-term mean.

We further decompose the velocity anomaly into a surface Ekman driven component, $v'_{Ek}(x,z,t)$ (calculated from the wind stress, with uniform compensating flow below the surface layer), and a remainder, $v''(x,t)$.

$$\Psi'_{\overline{\sigma}\,v'}(\sigma,m) = \Psi'_{\overline{\sigma}\,v'_{Ek}}(\sigma,m) + \Psi'_{\overline{\sigma}\,v''}(\sigma,m) \tag{22}$$

The density anomaly is decomposed in two ways, applied independently. Firstly, into a part due to temperature anomalies (with salinity held at the mean) σ'_T, a part due to salinity anomalies (with temperature held at the mean) σ'_S, and a part σ'_{TS} due to the non-linearities in the equation of state.

$$\Psi'_{\sigma'\,\overline{v}}(\sigma,m) \approx \Psi'_{\sigma'_T\,\overline{v}}(\sigma,m) + \Psi'_{\sigma'_S\,\overline{v}}(\sigma,m) + \Psi'_{\sigma'_{TS}\,\overline{v}}(\sigma,m)\,. \tag{23}$$

This equality is approximate because of the non-linearities in the velocity and density fields.

https://doi.org/10.5194/egusphere-2025-616
Preprint. Discussion started: 14 February 2025

Secondly, we decompose the density anomaly into a part due to zonally uniform density anomalies $\langle\sigma'\rangle$ and a remainder σ''.

$$\Psi'_{\sigma'\,\overline{v}}(\sigma,m) \approx \Psi'_{\langle\sigma'\rangle\,\overline{v}}(\sigma,m) + \Psi'_{\sigma''\,\overline{v}}(\sigma,m)\,. \tag{24}$$

The zonally uniform seasonal density anomaly term, $\langle\sigma'\rangle$, has little signal below 500 m. This decomposition was chosen in part because the zonally uniform density anomaly term has no spatial density gradients and is therefore independent of the geostrophic velocity field.

Finally, note that since MOC_σ and σ_{MOC} are functions of the maximum of the streamfunction Ψ_σ, we cannot calculate their anomalies directly from the anomalies in Eqs. 21 to 24. We must first add back in the long-term mean ($\overline{\Psi}_\sigma$) and then calculate the MOC_σ anomalies. For example, for the total anomaly:

$$\mathrm{MOC}'_\sigma\left(\Psi'_\sigma\right) = \mathrm{MOC}_\sigma\left(\Psi'_\sigma + \overline{\Psi_\sigma}\right) - \mathrm{MOC}_\sigma\left(\overline{\Psi_\sigma}\right) \tag{25}$$

We have described the decomposition in density space, but Eqs. 15 to 25 have exact parallels in temperature and salinity space which we will not detail here.

3 Results

We present the characteristics of the seasonal cycle at OSNAP obtained by applying the above density-space analysis to the 20-year model output. First we consider the full OSNAP section (Sect. 3.1.1), before separately examining $\mathrm{OSNAP_E}$ and $\mathrm{OSNAP_W}$ (Sect. 3.1.2), then we use the model results to aid interpretation of OSNAP observations (Sect. 3.2) and finally we look at heat and freshwater fluxes (Sect. 3.3).

The modelled mean overturning streamfunction in density space for the full OSNAP line ($\overline{\Psi_\sigma}$, Fig. 1g) shows the well-known, classic shape, with net northward flow at lower densities and net southward flow at higher densities. The modelled MOC_σ of the mean overturning, ($\max(\overline{\Psi_\sigma})$) is about 13 Sv and occurs at density $\sigma_{\mathrm{MOC}} = 27.55$. These values are both lower than found in the observational data (Fig. 2g), but the structure of the modelled streamfunctions is close enough to the observations to give confidence in the modelled overturning.

3.1 Modelled seasonal cycles

3.1.1 Full OSNAP section

The monthly overturning streamfunction anomalies ($\Psi'_\sigma(\sigma,m)$, Fig. 3a) have a dominant dipole structure in both density and time. At lower densities (less than about 27.4 $\mathrm{kg\,m^{-3}}$) positive overturning streamfunction anomalies peak in the autumn with negative anomalies peaking in spring. Conversely, at higher densities (greater than 27.4 $\mathrm{kg\,m^{-3}}$) positive streamfunction anomalies peak in the spring with negative anomalies peaking in autumn. The density of maximum overturning also varies through the year, as might be expected, with a maximum in spring when waters are densest after winter cooling, and minimum

https://doi.org/10.5194/egusphere-2025-616
Preprint. Discussion started: 14 February 2025

in autumn. Note that the density of maximum overturning does not coincide with the density where the largest streamfunction anomalies are found, so the seasonal cycle in MOC_σ Fig. 3f, which approximately samples the anomalies at density σ_{MOC} (green line in Fig. 3b), mostly samples the higher densities but misses the extremes of the seasonal cycle at both higher and lower densities. The density flux (Fig. 3j), the integral in density of the overturning streamfunction anomalies, shows maximum southward density flux (largest negative values) in June and minimum in January, lagging 2 to 3 months behind the meridional overturning seasonal signal.

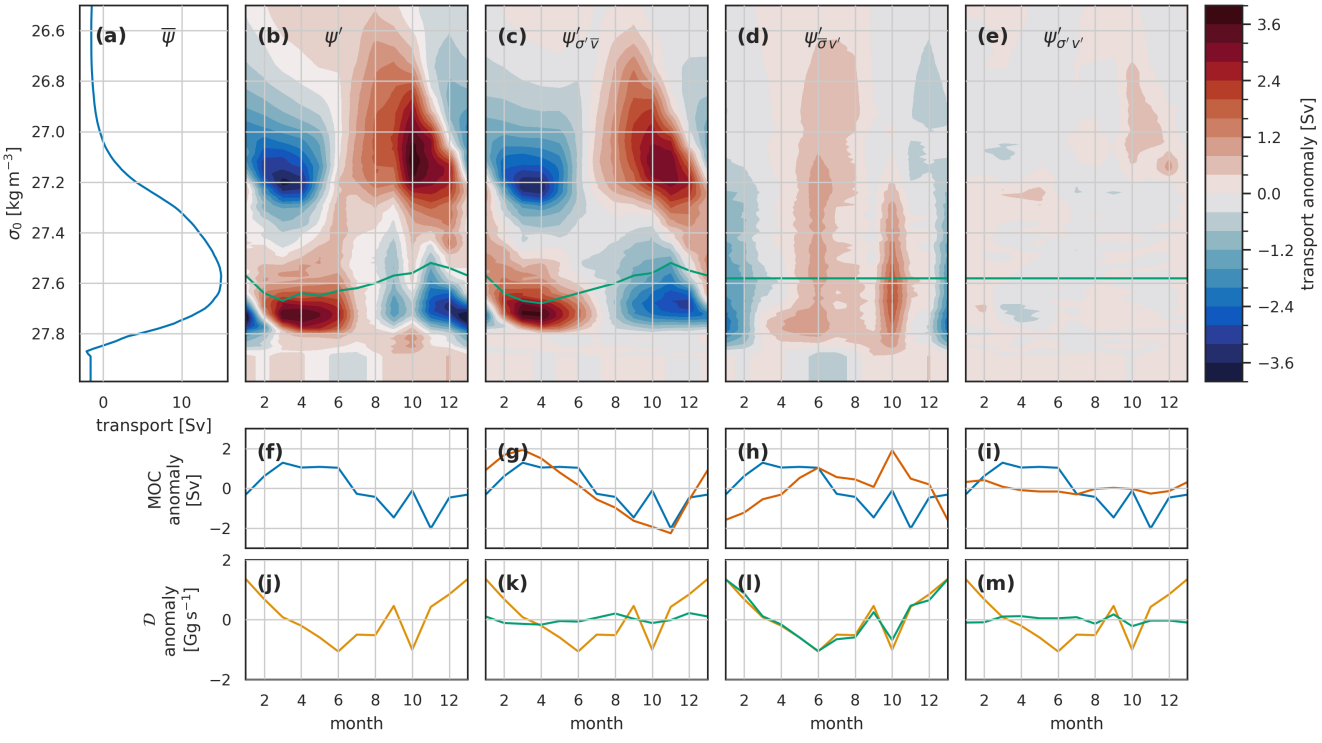

Figure 3. The seasonal cycle in the overturning streamfunction (Ψ), MOC and density flux ($\mathcal{D}$) for the full OSNAP transect in the Viking20x model. (a) the mean overturning streamfunction. (b-e) Hovmöller (time – σ) plots of seasonal streamfunction anomalies. The green line in each shows the associated variability of σ_{MOC}. The plots are arranged in columns: (b,f,j) the full anomalies, (c,g,k) the anomalies associated with density variations and mean velocities, (d,h,l) velocity variations and mean density, (e,i,m) velocity and density co-variation. The lower two rows are MOC (f-i) and density flux $\mathcal{D}$ (j-m). In (g-i) the blue line is for the total anomalies, copied across from panel (f), while the orange line is the respective anomaly component. Similarly, the yellow, total anomaly line in (j) is repeated in panels (k-m) alongside the green line showing the respective components of density flux anomaly.

We now decompose the overturning streamfunction anomalies into separate parts driven by seasonality in density and velocity (Eq. 21, Fig. 3c-e). The dipole structure occurs in the anomalies associated with density variability ($\Psi'_{\sigma'\overline{v}}(\sigma, m)$, Fig. 3c). The seasonal cycle at lighter densities, with its peak in autumn, is caused by the seasonal cycle in density of northward flowing water. The cycle is reversed for denser waters, with peak positive overturning streamfunction anomalies

https://doi.org/10.5194/egusphere-2025-616
Preprint. Discussion started: 14 February 2025

in spring, because denser waters flow predominantly southward. The seasonal velocity variability drives a different pattern of overturning streamfunction variability, with consistent sign across almost the whole density range ($\Psi'_{\overline{\sigma}\,v'}(\sigma, m)$, Fig. 3d). This annual cycle has its minimum in January and peaks in July, with a secondary, sharp, peak in October. This pattern corresponds with an increase in net inflow of lighter waters in phase with a net outflow of denser waters. The streamfunction variability associated with co-variance of velocity and density is everywhere small ($\Psi'_{\sigma' v'}(\sigma, m)$, Fig. 3e).

The resulting seasonal variability in the meridional overturning (Fig. 3f-i) is mostly due to the seasonal density variation (Fig. 3g), and in particular the seasonal density variation of denser waters. The velocity variation acts mostly to delay the MOC seasonal peak and introduce some higher-frequency variability in the autumn. In contrast, the seasonal northward density flux anomalies (Fig. 3j-m) are almost entirely due to the velocity variability (Fig. 3l).

Decomposing the overturning streamfunction further, beginning with the velocity-driven component (Fig. 4), we find the dominant factor to be the seasonal cycle in surface Ekman transport. This produces seasonal overturning streanmfunction variability with a maximum in summer minimum in winter. The timing is due to the surface Ekman transport being generally southward, opposing the overturning. The summer maximum corresponds to a minimum in this opposition. The streamfunction variability shows as a summer MOC maximum and northward density flux minimum (i.e. southward maximum). The remainder again shows a narrow peak overturning streamfunction anomaly in the autumn, we have been unable to discover the precise cause of this but it appears to be located in the barotropic transport variability. The shorter, 6-year, model results show a stronger seasonal cycle driven by the barotropic velocity variability (Fig. S1c) suggesting interannual variability of the seasonal cycle.

Turning to the density-driven component, we decompose this in two independent and complementary ways. First separating out the component associated with zonal mean seasonal cycle of density, and secondly into two components due to temperature and salinity variations. The zonal mean seasonal cycle of density is almost entirely confined to the surface 500 m (Fig. 5), and accounts for almost all the density-driven variability in MOC and most of that in the overturning streamfunction (Fig. 6). The domination of the zonal mean density signal in MOC variability is due to the seasonal cycle of summer/autumn lighter surface densities and winter/spring denser surface waters in the near-surface southward flow. This southward flow occurs primarily in the East Greenland Current and Labrador Current. Because much of the East Greenland Current flows back northwards as the West Greenland Current much of that transport cancels, leaving the OSNAP-wide seasonal MOC variability largely dominated by near-surface density changes in the Labrador Current.

Further exploration of the variability in the streamfunction remainder (Fig. 6d) shows the lower-density remainder (centred at 27.2 $\mathrm{kg\,m^{-3}}$) to be due to the zonal mean underestimating seasonal mixed layer depth and density variability in the North Atlantic Current in the east of the section. The remainder at higher densities (centred at 27.7 $\mathrm{kg\,m^{-3}}$) is similarly due to underestimation of the seasonal cycle of isopycnal depth in the Labrador Current outflow. These remainders have no expression in the MOC because of the density at which they occur. The two effects largely cancel in the density flux metric, this appears to be by chance and not true for the separate $\mathrm{OSNAP_E}$ and $\mathrm{OSNAP_W}$ calculations below. Note that the isopycnal depth change in the Labrador Current outflow is the only notable seasonal influence we see on the overturning streamfunction from below 500 m, here down to 800 – 1000 m.

https://doi.org/10.5194/egusphere-2025-616
Preprint. Discussion started: 14 February 2025

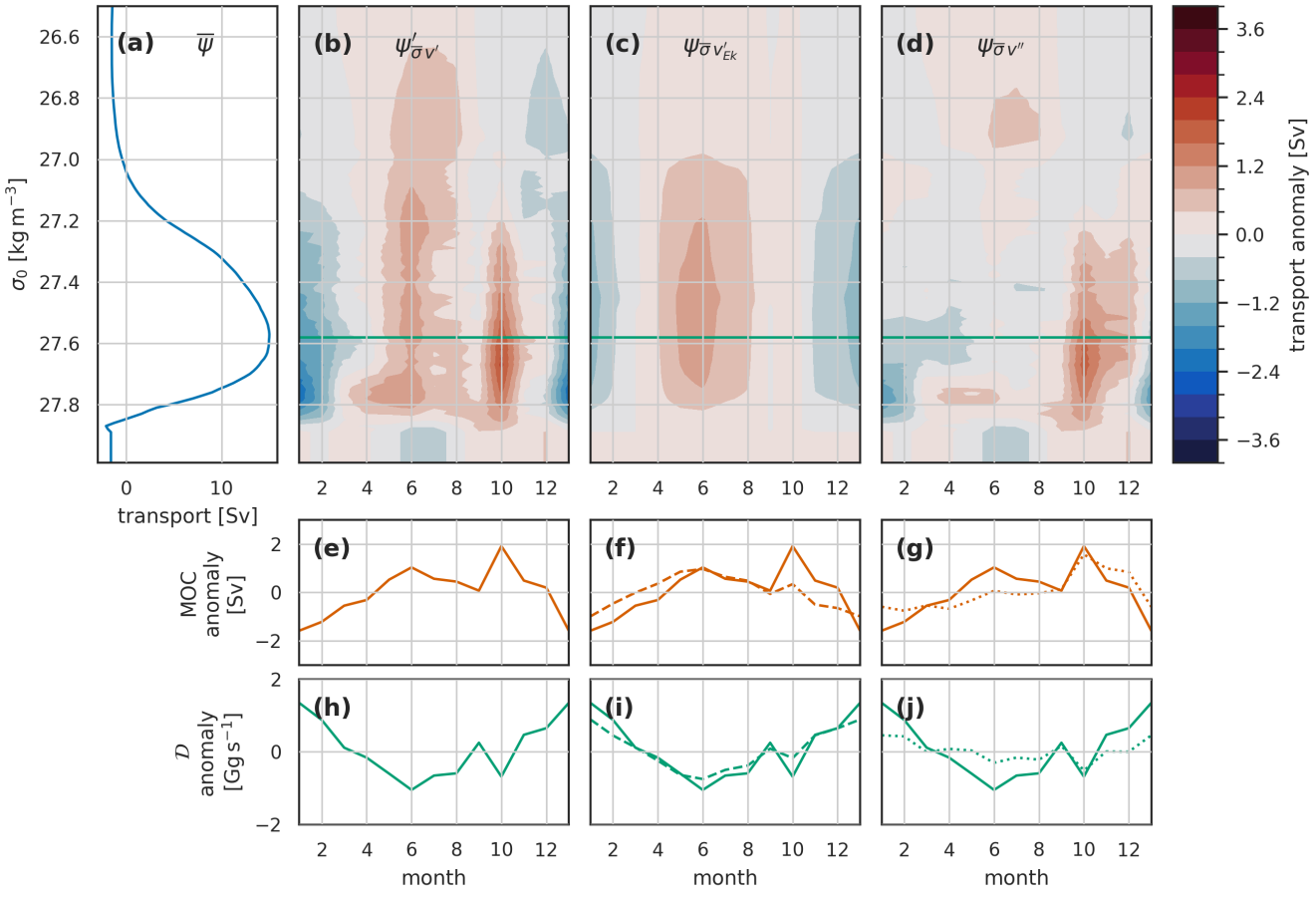

Figure 4. The seasonal cycle due to velocity variability (constant mean density structure) in the overturning streamfunction (Ψ), MOC and density flux ($\mathcal{D}$) for the full OSNAP transect in the Viking20x model. (a) the mean overturning streamfunction. (b-d) Hovmöller (time – σ) plots of seasonal streamfunction anomalies. The green line in each shows the associated variability of σ_{MOC}. The plots are arranged in columns: (b,e,h) the full velocity-driven anomalies, (c,f,i) velocity-driven anomalies associated with Ekman surface velocity variability, and (d,g,j) the anomalies associated with the remainder of the velocity variability. The lower two rows are MOC (e-g) and density flux $\mathcal{D}$ (h-j). In (f,g) the solid orange line is for the total velocity-driven MOC anomalies, copied across from panel (e); the dashed line in (f) is the Ekman driven MOC anomaly; and the dotted line in (g) is the remainder-driven MOC anomaly. Similarly, the solid green total density flux anomaly line in (h) is repeated in panels (i,j) alongside the dashed line in (i) showing the Ekman driven $\mathcal{D}$ and the dotted line in (j) is the remainder-driven $\mathcal{D}$ anomaly.

Finally we examine the separate contributions of seasonal temperature and salinity variability to the density-driven seasonal cycle (Fig. 7). The seasonal cycle in the overturning streamfunction is dominated by temperature variability, with the influence of salinity variability mostly confined to the upper limb where it generally opposes the temperature variability (Fig. 7b-d). While the seasonal cycle in the overturning streamfunction is dominated by temperature variability, both MOC and density

https://doi.org/10.5194/egusphere-2025-616
Preprint. Discussion started: 14 February 2025

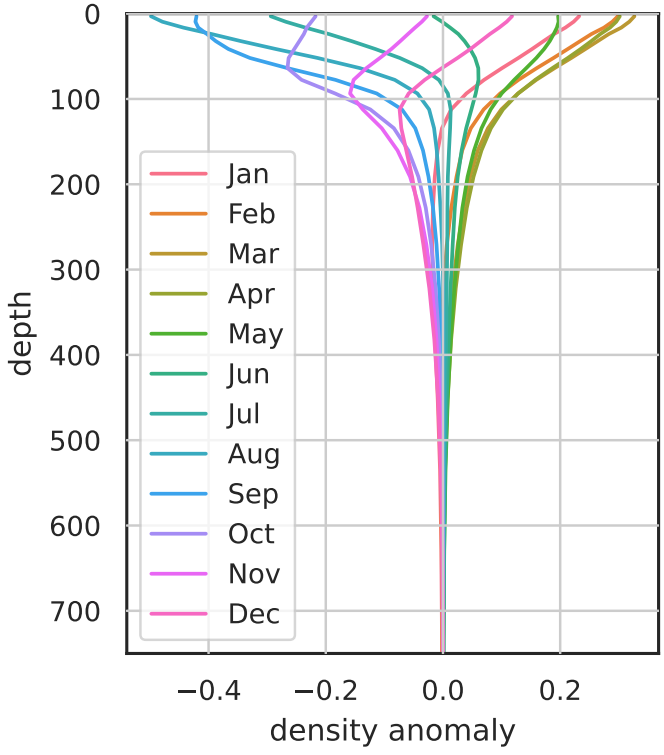

Figure 5. Seasonal cycle in the Viking20x model zonal mean density anomalies. Note that the zonal mean seasonal density variability is largely confined to the surface 200 m, and almost entirely confined to the surface 500 m. The maximum positive seasonal anomalies (densest surface waters) are found in March-April at all depths, the maximum negative anomalies (lightest waters) are found between August and December depending on depth. The deeper layers lag the surface layers in seasonal minimum densities.

flux seasonal cycles have fairly equal contributions from temperature and salinty variability. This is bacause sampling at the maximum of the streamfunction for MOC does not capture the maximum temperature-driven anomalies, and integrating the anomalies in density space for the density flux involves cancellation of the large positive and negative temperature-driven anomalies (Fig. 7c,f,i). The salinity-driven anomalies however, with a simpler single peaked form in density, are more efficiently expressed in both MOC and density flux (Fig. 7d,g,j).

The opposition between temperature and salinity anomalies at lower densities is seen in the density flux anomalies (Fig. 7h-j) where temperature and salinity contributions to the density flux largely cancel producing no net density-driven density flux anomalies. However, because of the distribution of streamfunction anomalies in density space with respect to σ_{MOC} the influence of temperature and salinity on MOC are in phase, both temperature and salinity driving the spring MOC maximum (Fig. 7e-g). It is worth noting that the temperature-driven anomalies drive stronger late winter/spring MOC but weaker southward density flux. While both MOC and density flux seasonal cycles are dominated by the surface waters, temperature-driven density flux anomalies are dominated by the seasonal cycle in the lighter northward-flowing waters while

https://doi.org/10.5194/egusphere-2025-616
Preprint. Discussion started: 14 February 2025

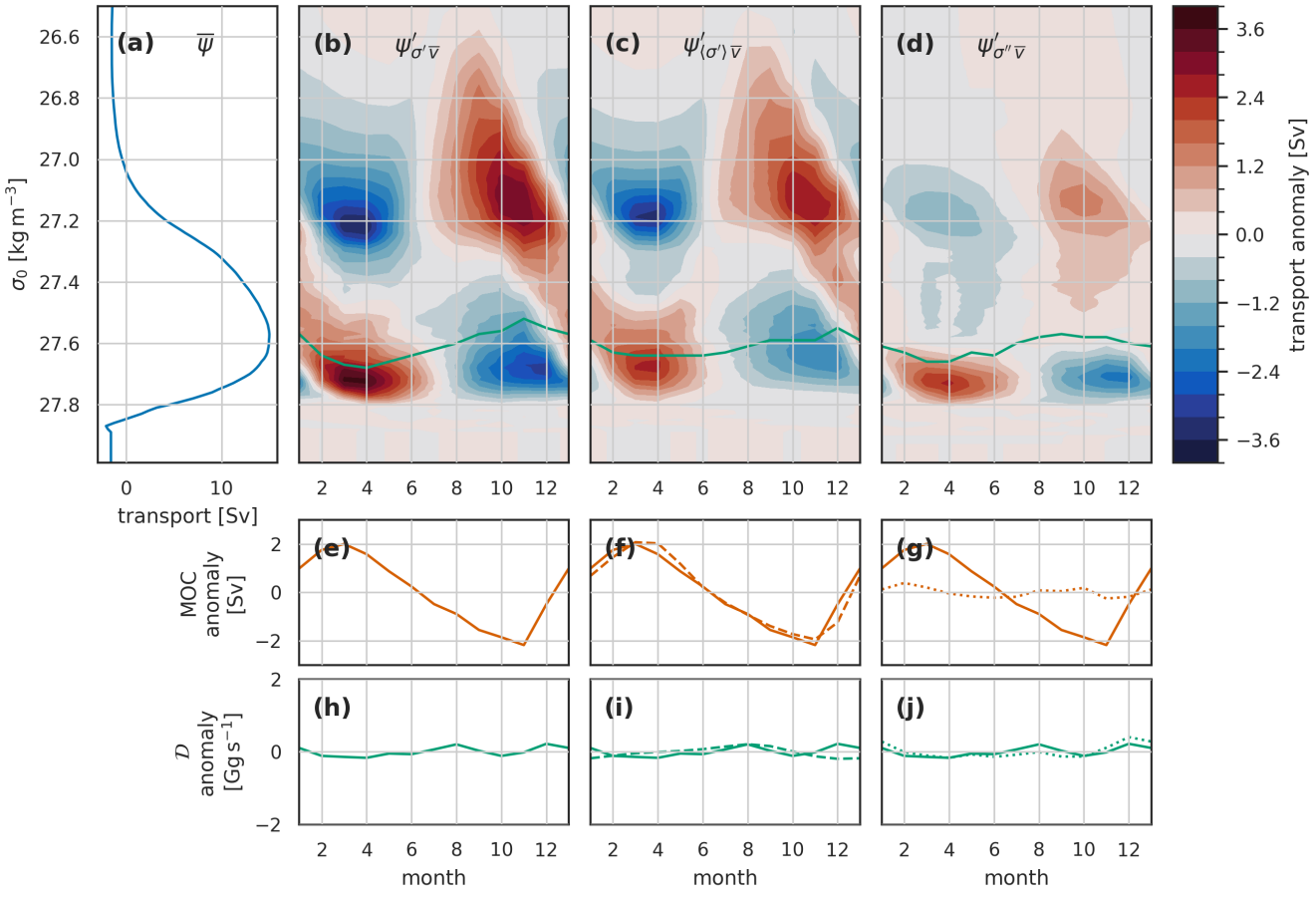

Figure 6. Similar to Fig. 4 but for the seasonal cycle due to density variability (constant mean velocity structure) in the overturning streamfunction (Ψ), MOC and density flux ($\mathcal{D}$) for the full OSNAP transect in the Viking20x model. This figure has the same structure as Fig. 4 but the columns here refer to: (b,e,h) the full density-driven anomalies, (c,f,i) density-driven anomalies associated with zonal mean density variability, and (d,g,j) the anomalies associated with the remainder of the density variability.

temperature-driven MOC anomalies are dominated by variability in the southward-flowing waters at the western boundaries where the σ_{MOC} isopycnal is close to the surface.

To aid comparison with the seasonal cycles of MOC and density flux for $\mathrm{OSNAP_E}$ and $\mathrm{OSNAP_W}$ and in the OSNAP observational data we bring together the MOC and density flux plots from Figs. 4, 6 and 7 in Fig. 8.

3.1.2 OSNAP East and OSNAP West

The seasonal cycles of MOC and density flux on the individual $\mathrm{OSNAP_E}$ (Fig. 9) and $\mathrm{OSNAP_W}$ (Fig. 10) sections bear many similarities to the full section (Fig. 8). In all cases the seasonal cycle of the overturning circulation, MOC, is dominated by the

https://doi.org/10.5194/egusphere-2025-616
Preprint. Discussion started: 14 February 2025

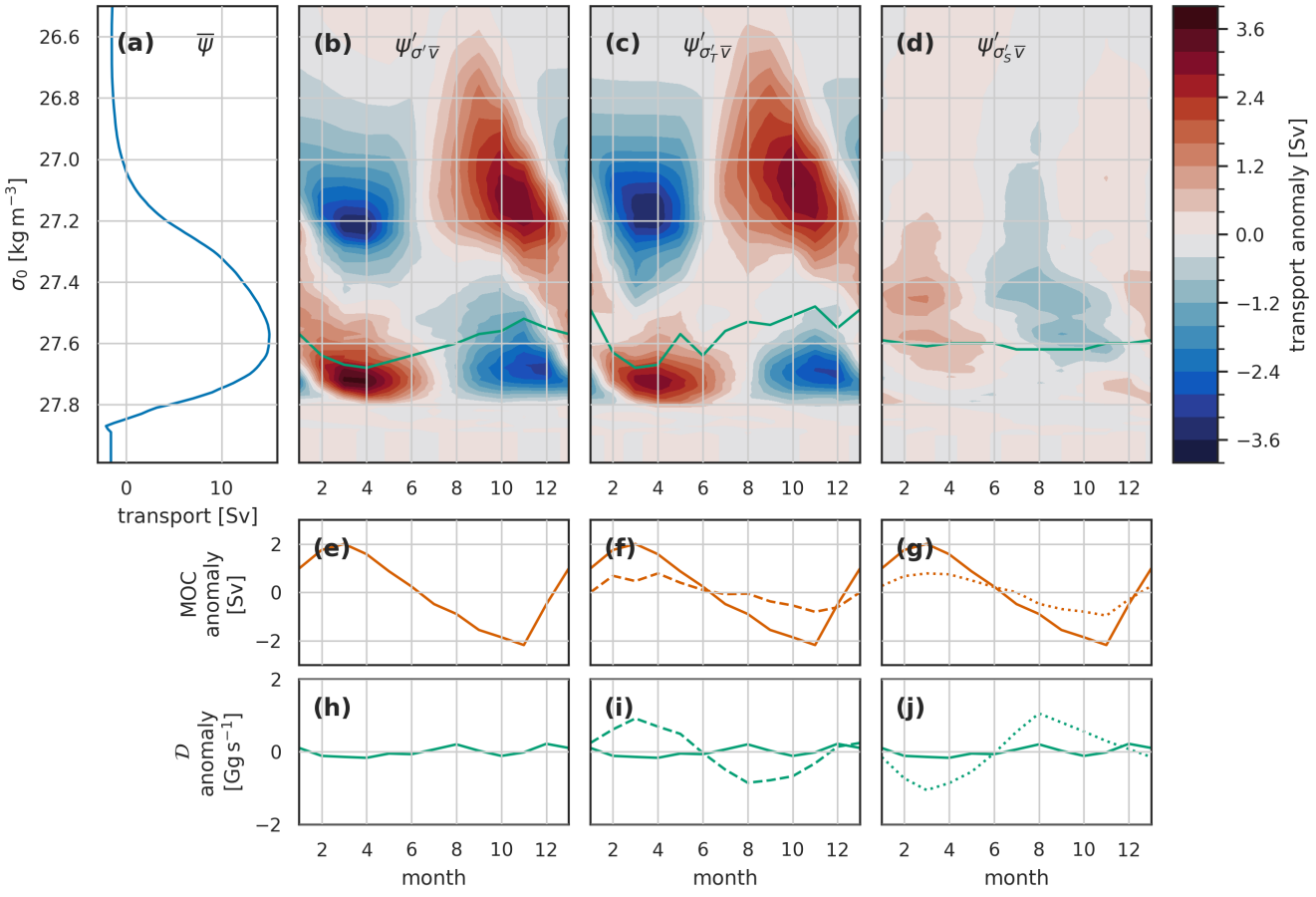

Figure 7. Similar to Fig. 6 but for the decomposition of the seasonal cycle due to density variability into separate components driven by temperature and salinity variability. This figure has the same structure as Fig. 6 but the columns here refer to: (b,e,h) the full density-driven anomalies, (c,f,i) density-driven anomalies associated with temperature variability, and (d,g,j) the anomalies associated with salinity variability.

density variation, and specifically by the seasonal cycle of density in the southward surface flow at the western boundary. The Ekman contribution is largely confined to $OSNAP_E$, this is as expected due to the orientation of the prevailing wind vectors eastward along $OSNAP_E$ (driving surface flow southward across the section) but across $OSNAP_W$ driving along-section flow which does not contribute to overturning.

Perhaps the most notable difference between the full OSNAP section and both $OSNAP_E$ and $OSNAP_W$ is that while the density-driven seasonal density flux anomalies across OSNAP was small (Fig. 8d,e) they are a significant factor in the seasonal cycles at both $OSNAP_E$ and $OSNAP_W$. The $OSNAP_E$ and $OSNAP_W$ cancel when considering the full section. This cancellation is largely explained by variability associated with the East Greenland Current flowing southward across $OSNAP_E$ being strongly correlated with that of the West Greenland Current flowing northward across $OSNAP_W$.

https://doi.org/10.5194/egusphere-2025-616
Preprint. Discussion started: 14 February 2025

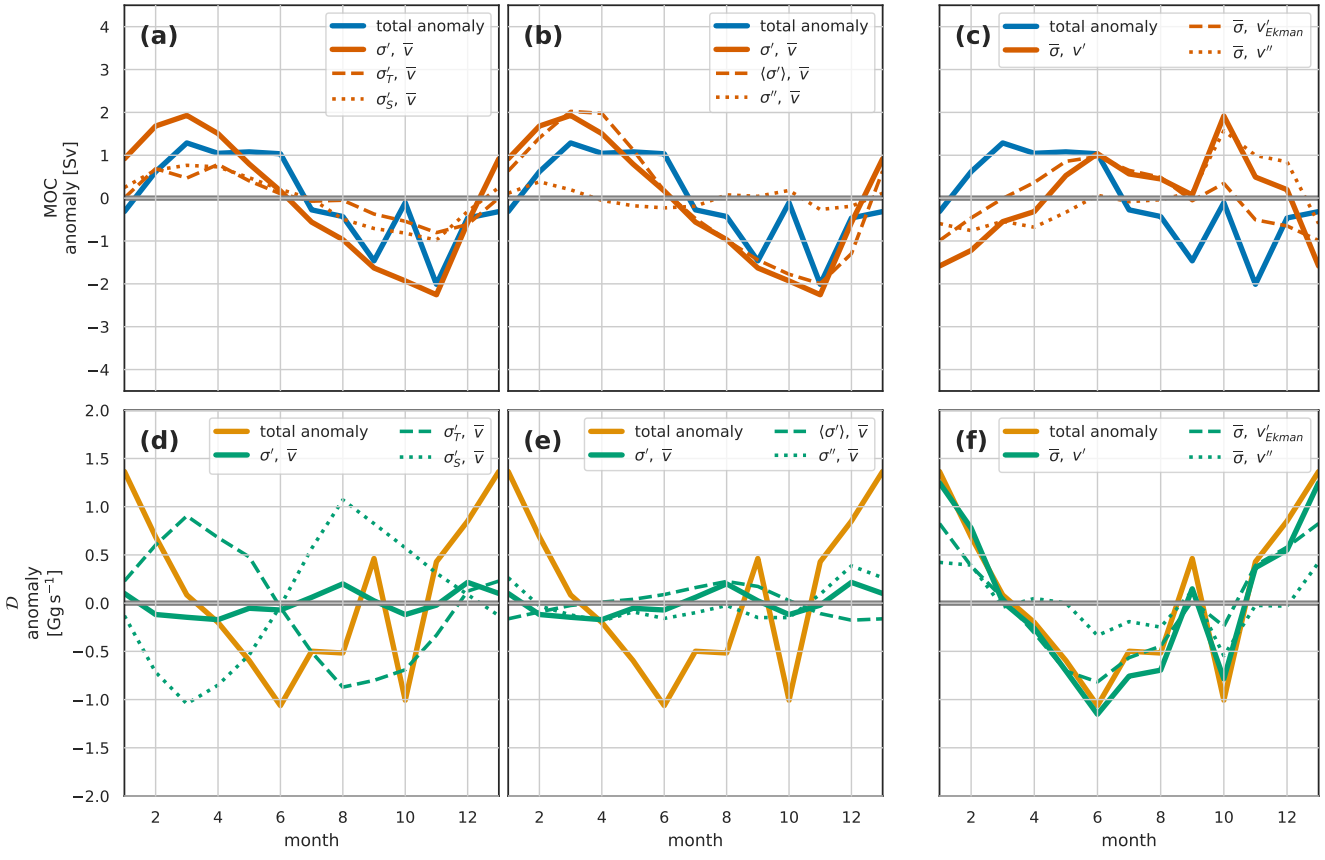

Figure 8. Summary plot of the decomposition of the seasonal cycle for the **full OSNAP section** of (a-c) MOC_σ and (d-f) density flux $\mathcal{D}$ for the **Viking20x model**. The left-hand column (a,d) shows the density-driven decomposition into temperature and salinity components; the middle column the density-driven decomposition into zonal mean and remainder; and the right-hand column the velocity-driven decomposition into Ekman and remainder components. The blue line repeated in (a-c) is the total MOC_σ anomaly; the solid orange line is either the total density-driven anomaly component of MOC_σ (a,b), or the total velocity-driven component (c). The dashed and dotted lines in (a-c) are respectively: in (a) the temperature and salinity driven components; in (b) the zonal mean density and density-driven remainder components; and in (c) the Ekman driven and velocity-driven remainder components. Similarly, for (d-f) the repeated yellow line is the total $\mathcal{D}$ anomaly; the solid green line is either the total density-driven anomaly component of $\mathcal{D}$ (d,e), or the total velocity-driven component (f). The dashed and dotted lines in (d-f) are respectively: in (d) the temperature and salinity driven components; in (e) the zonal mean density and density-driven remainder components; and in (f) the Ekman driven and velocity-driven remainder components. Several of the figures following share this format so it is worth spending a moment to understand it.

Compared to the full OSNAP section (Fig. 8), $\mathrm{OSNAP_E}$ shows more domination of both MOC and density flux seasonal cycles by temperature variability (Fig. 9a,d), with the salinity component confined almost entirely to $\mathrm{OSNAP_W}$. $\mathrm{OSNAP_E}$

https://doi.org/10.5194/egusphere-2025-616
Preprint. Discussion started: 14 February 2025

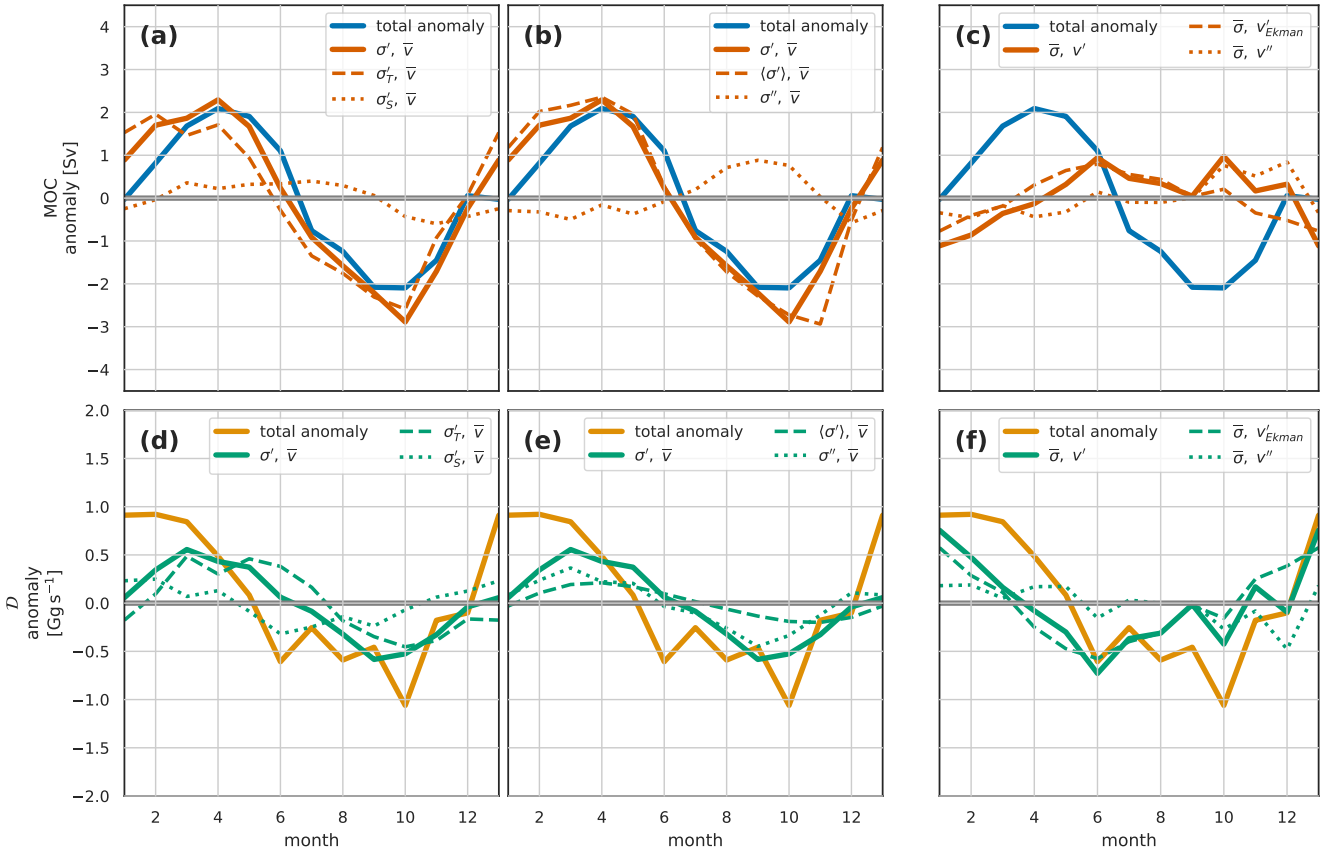

Figure 9. As for Fig 8 but for the **Viking20x model** seasonal cycle at **OSNAP$_E$**.

seasonal temperature variability is also the source of the slightly counterintuitive result where enhanced MOC is associated with weaker southward density flux.

As for the full section, in OSNAP$_W$ temperature- and salinity-driven seasonal variability reinforce each other for MOC but are opposed for density flux (Fig. 9a,d). The salinity signal here dominating the density-driven density flux. The density-driven density flux in turn dominates the total density flux at OSNAP$_W$.

In the full section, the decomposition of density-driven variability into zonal-averaged seasonal cycle and a remainder (Fig. 6) neatly resulted in no residual contribution to either MOC or density flux, though some variability is seen in the residual streamfunction (Fig. 6d). This residual streamfunction variability is made of two spatially separate contributions: the contribution at lighter densities is due to the zonal mean seasonal cycle underestimating the seasonal cycle in the North Atlantic Current in the eastern part of OSNAP$_E$; while the contribution at higher densities is due to the zonal mean underestimating the seasonal cycle of isopycnal heave in the Labrador current outflow across OSNAP$_W$. This residual contribution is the key factor

https://doi.org/10.5194/egusphere-2025-616
Preprint. Discussion started: 14 February 2025

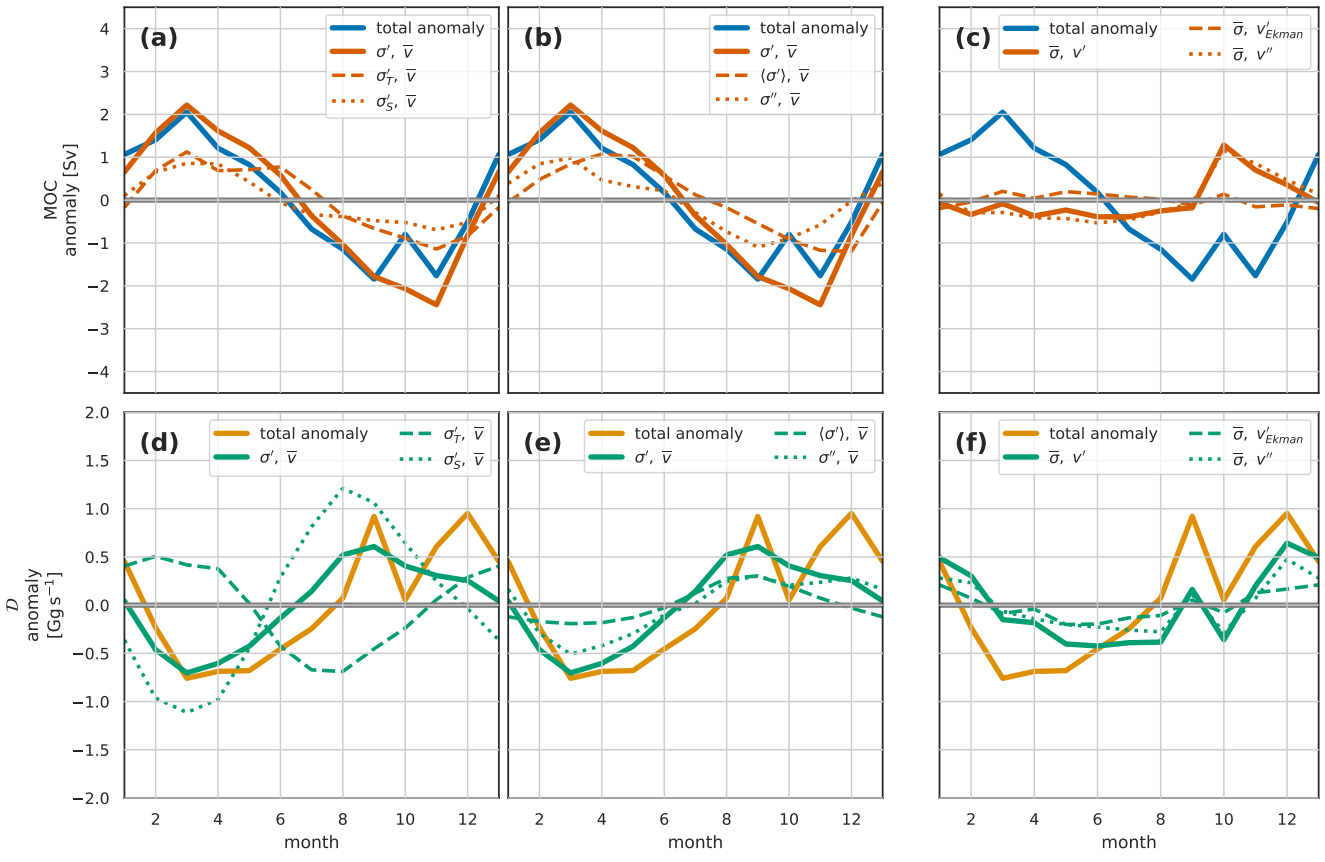

Figure 10. As for Fig 8 but for the **Viking20x model** seasonal cycle at **OSNAP$_W$**

in the larger contribution of density-driven anomalies to the seasonal cycle of density flux in both OSNAP$_E$ and OSNAP$_W$ when compared to the full OSNAP section.

285 It should be noted that while the density fluxes in OSNAP$_E$ and OSNAP$_W$ sum to the full OSNAP density fluxes the same does not hold for MOC as σ_{MOC} is significantly denser in OSNAP$_W$ than OSNAP$_E$.

3.2 Observed seasonal cycles

3.2.1 Full OSNAP section

The mean seasonal cycle of the overturning streamfunction (Fig. 11a) in the observations is very similar to the model (Fig. 3a)
290 though with the peak overturning at a slightly higher density.

Comparing the observed seasonal cycle of the streamfunction (Fig. 11b-d) with the model (Fig. 3b-d) highlights many similarities but also notable differences. Perhaps most noticeable is the higher levels of high-frequency (month-to-month rather than seasonal) variability in the observations compared to the model. This high frequency signal is dominated by the

https://doi.org/10.5194/egusphere-2025-616
Preprint. Discussion started: 14 February 2025

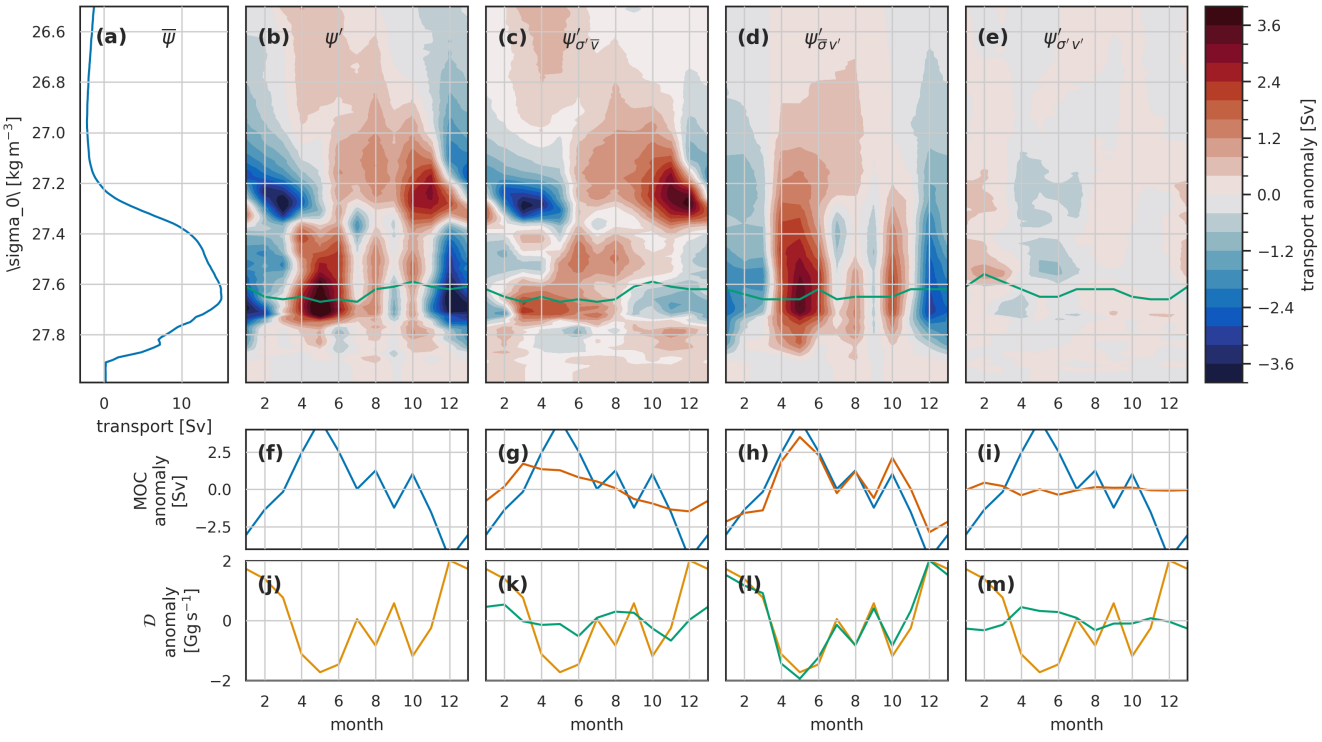

Figure 11. The seasonal cycle in the (a-e) overturning streamfunction Ψ, (f-i) MOC, and (j-m) density flux $\mathcal{D}$ for the full OSNAP transect in the **OSNAP observations**. Seasonal total anomalies (b,f,j) are decomposed into (c,g,k) density-driven, (d,h,l) velocity-driven and (e,i,m) covarying density-velocity components. See Fig. 3 for full details of the figure layout.

velocity-driven component. This disparity is partly due to the shorter time period analysed in the observations (6 years as against 20 years in the model). To test this we repeated the model analysis using purely the 2014 to 2020 period to match the observations. While this produced a larger high-frequency signal than the 20 year model run it was still notably smaller than that in the observations and partly obscured the model signal, a subset of these results 6 year model results are presented in the Supplementary Information, Figs. S1-S3.

Looking past this high-frequency signal to the seasonal signal we again see the dipole structure described in the model (Fig. 11b), though not as well-defined. At lower densities this is dominated by the density-driven anomalies (Fig. 11c) and in particular by the zonal mean near-surface density-driven anomalies (not shown). At higher densities, above and around the density of maximum overturning, this density-driven seasonal cycle (Fig. 11c) is somewhat weaker in the observations than in the model.

The velocity-driven anomalies are stronger in the observations (Fig. 11d) than in the model (Fig. 3d), with a particularly strong maximum centred in May which is not really present in the modelled anomalies. This May maximum is mostly in the residual component, and is part of the higher-frequency signal described above.

https://doi.org/10.5194/egusphere-2025-616
Preprint. Discussion started: 14 February 2025

The generally weaker density-driven and stronger velocity-driven seasonal cycles in the observed overturning streamfunction are reflected in the meridional overturning (Fig. 11f-i) and density flux (Fig. 11j-m). Whereas in the model the density-driven component was the largest component of MOC_σ, in the observations the velocity-driven component is dominating both MOC and density flux.

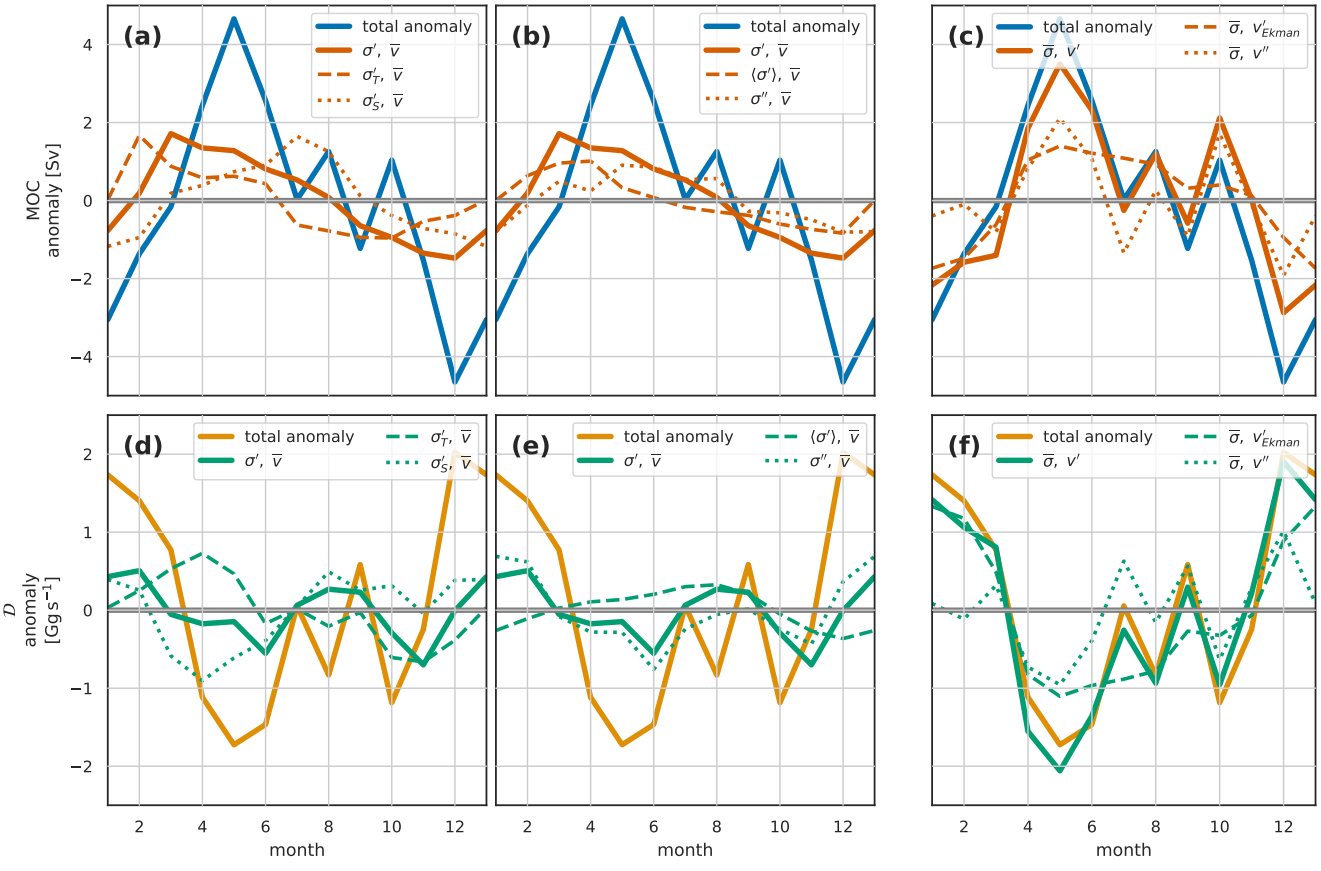

Figure 12. As for Fig 8 but for the **observed** seasonal cycle on the **full OSNAP section**.

Figure 12 breaks down the observed MOC and density flux into the various components (compare with Fig. 8). The observed MOC seasonal cycle, in contrast to the model, is dominated by the velocity-driven anomalies. These anomalies are a combination of the annual cycle of surface Ekman-driven flows, with a minimum in the winter when the stronger wind-driven Ekman currents oppose the overturning, and residual flows. These residual flows, generally showing higher-frequency variability, are notably larger in the observations than in the model. The density-driven part of the observed MOC seasonal cycle, as for the model, shows contributions from both temperature and salinity variability (Fig. 12a), though the observed variability due to salinity is shifted out of phase (lagging by 4 to 5 months). The density-driven MOC variability (Fig. 12b) has a larger contribution from the residual component than in the model.

https://doi.org/10.5194/egusphere-2025-616
Preprint. Discussion started: 14 February 2025

The observed density flux seasonal cycle, as with the model, is dominated by the velocity driven variability (Fig. 12f), though with generally larger contribution from the residual component than in the model. The density-driven component of the observed density flux seasonal cycle is relatively small and variable with no clearly dominant components (Fig. 12d,e). As for the model, the observed density flux seasonal cycle shows some opposition between temperature and salinity-driven signals.

3.2.2 OSNAP East and OSNAP West

For $\mathrm{OSNAP_E}$, as for the full section, velocity-driven variability dominates both MOC and density flux seasonal cycles (Fig. 13). This velocity variability is a combination of seasonally varying Ekman transports and a high-frequency remainder. Though it forms the smaller part of the seasonal cycle, we look now at the density-driven variability in more detail. A particular feature of the seasonal cycle of observed density-driven MOC in $\mathrm{OSNAP_E}$, which isn't seen in the full OSNAP section, $\mathrm{OSNAP_W}$ or the model, is the opposing contribution of temperature and salinity (Fig. 13a). We examine this in Fig. 14 where we plot the difference between the early spring and early autumn extremes of the seasonal cycle. The difference in density-driven MOC between these two extremes is purely due to the volume transport in the region between the respective σ_{MOC} isopycnals. Thus, we find the seasonal cycle of density-driven MOC in $\mathrm{OSNAP_E}$ to be almost entirely due to seasonal changes of near-surface density in the Irminger Basin; a competition between northward transports in the eastern basin driving an autumn peak in MOC (more northward flow in the lower limb reducing MOC in spring) and southward transports in the East Greenland Current at the west of the basin driving a spring peak. This competition is 'won' by the southward flows, resulting in the observed spring peak.

Panels b,c,d of Fig. 14 illustrate how the density-driven seasonal cycle of σ_{MOC} depth, and hence of MOC, is associated with the zonal-mean seasonal cycle of surface density in the Irminger Basin. This is primarily driven by large-scale seasonal temperature variation. Over much of the Irminger Sea the seasonal signal of near-surface salinity supports the temperature variation, reducing density by the autumn through seasonal heating and freshening. The dominant opposing salinity-driven signal in Fig. 13a is more subtle, and is due to a small region at the west of the section where the near-surface seasonal cycle of salinity is reversed, with warm salty water present in the autumn. This dominates the salinity-driven seasonal cycle because of the strong southward currents. This feature is also present in the model but lies mostly outside the region enslosed by the seasonal variation of σ_{MOC}. This more detailed analysis of the observed density-driven MOC at $\mathrm{OSNAP_E}$ highlights how variability in the measure of meridional overturning can be dominated by very local changes in regions of strong flow.

Observations of MOC and density-flux at $\mathrm{OSNAP_W}$ (Fig. 13d-f) show generally smaller amplitude and less coherent seasonal signal than in model. Velocity-variation is dominant, as in all the observations, even with small Ekman contribution. The observed seasonal cycle of density flux again shows opposing temperature and salinity components as for the observed full OSNAP section and the model. This opposition is a different mechanism to that for the $\mathrm{OSNAP_E}$ MOC seasonal cycle described above as the density-driven density-flux variability samples the full density fields, not just the region bounded by extremes of σ_{MOC}. As described previously, this opposition of temperature and salinity in the density flux seasonal cycle is due to the temperature component being dominated by the seasonal heating and cooling in northward-flowing surface waters,

https://doi.org/10.5194/egusphere-2025-616
Preprint. Discussion started: 14 February 2025

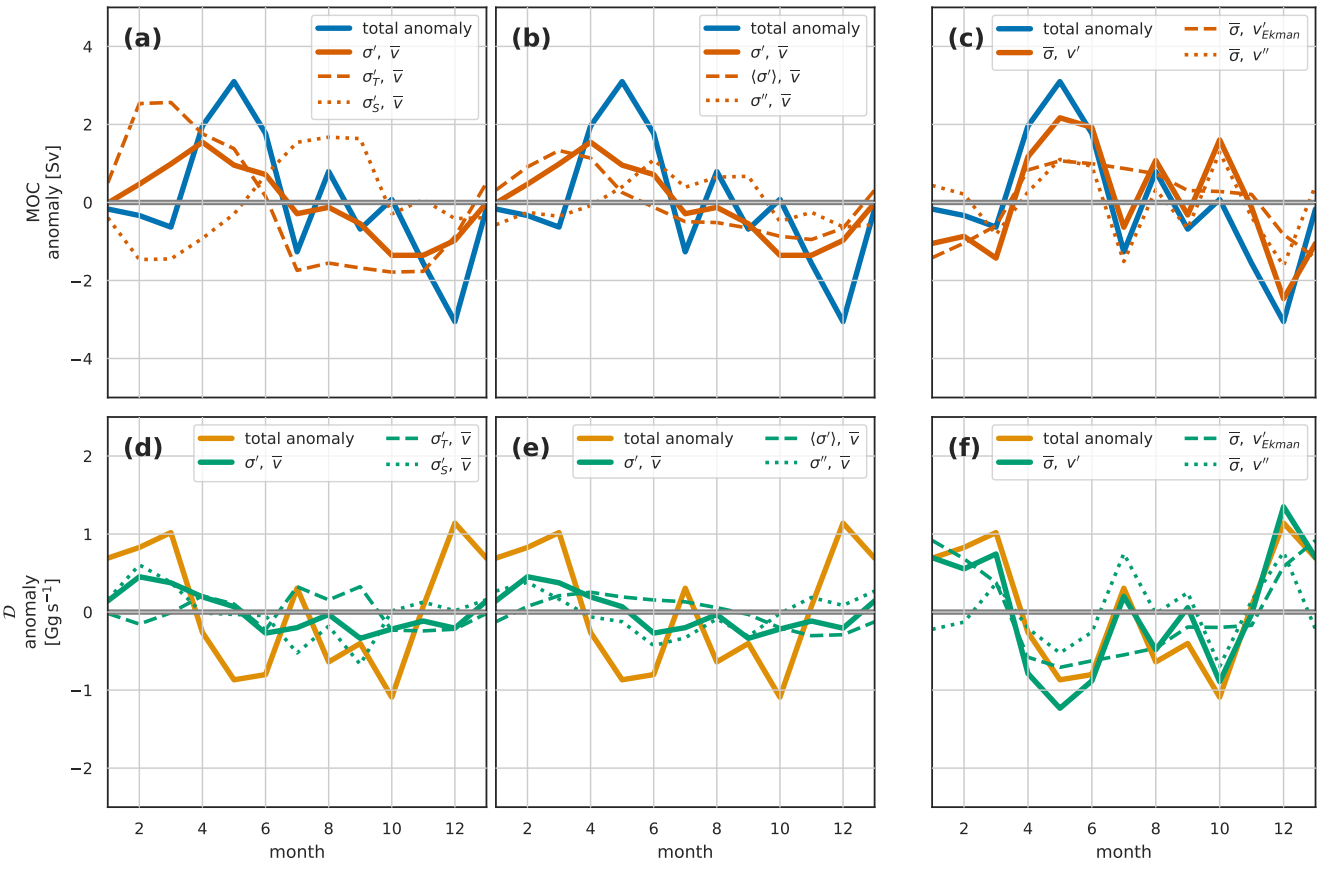

Figure 13. As for Fig 8 but for the **observed** seasonal cycle at **OSNAP$_E$**.

while the strong seasonal summer freshening of the southward surface flow on the western boundary dominates the salinity component.

3.3 Seasonal cycles of heat and freshwater transport

We might expect, with small net throughflow, that the density fluxes (Figs. 8d-f and 12d-f) would be some form of weighted sum of the heat and freshwater fluxes (with sign reversed). This relationship is not immediately obvious from the heat and freshwater fluxes for either the model (Fig. 16) or observations (Fig. 17).

Closer examination suggests that the fundamental shape of the seasonal cycle of density flux is being dominated by the freshwater flux. Both density and freshwater flux are predominantly southward through the year, the winter mimimum and spring-summer maximum in southward density flux correspond to winter maximum and spring-summer minimum in southward freshwater flux. The heat flux plays a more minor role, shifting the peak in the density flux and, particularly in the observational case, adding higher frequency variability. The principle complicating factor in relating heat and freshwater flux to density flux

https://doi.org/10.5194/egusphere-2025-616
Preprint. Discussion started: 14 February 2025

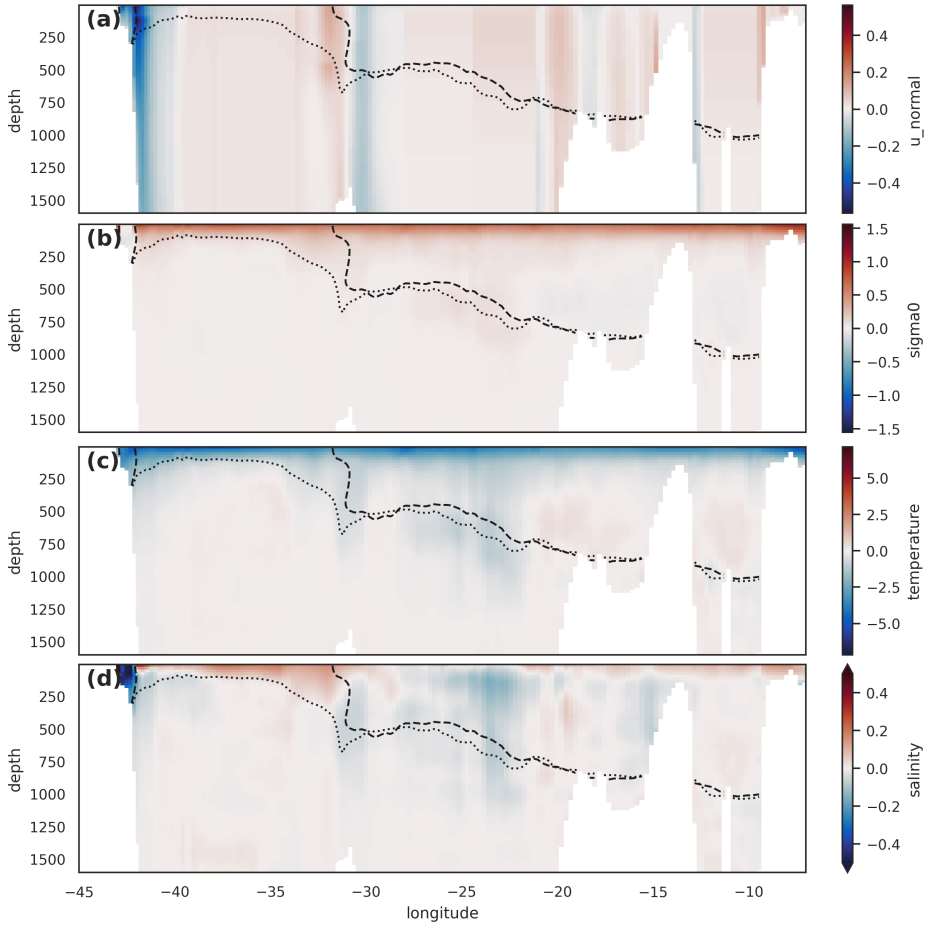

Figure 14. Observed OSNAP_E density-driven seasonal cycle. (a) mean velocity normal to the section, with σ_{MOC} for April (dashed line) and October (dotted line) superimposed. These represent the observed extremes of the density-driven seasonal cycle of σ_{MOC}. (b,c,d) show the difference between water properties in April and October (shading,April minus October) for (a) density, (b) temperature and (c) salinity. The σ_{MOC} for April (dashed line) and October (dotted line) are superimposed in each case.

is the large variability of the thermal expansion coefficient with temperature – at low temperatures the same amount of added heat causes a much smaller change in density than at higher temperatures.

Examining the decomposition of heat transports into components driven by the seasonal cycle of temperature and velocity (Figs. 16a,b and 17a,b) we find that, as for density, the seasonal cycle of transports is dominated by the velocity variability. But, whereas for density the dominant velocity variability is surface Ekman, for heat transport the seasonal variability is dominated by the remainder term, predominantly variability in the barotropic flow. In the observations this barotropic velocity variability is also the source of the high-frequency variability in heat transport.

https://doi.org/10.5194/egusphere-2025-616
Preprint. Discussion started: 14 February 2025

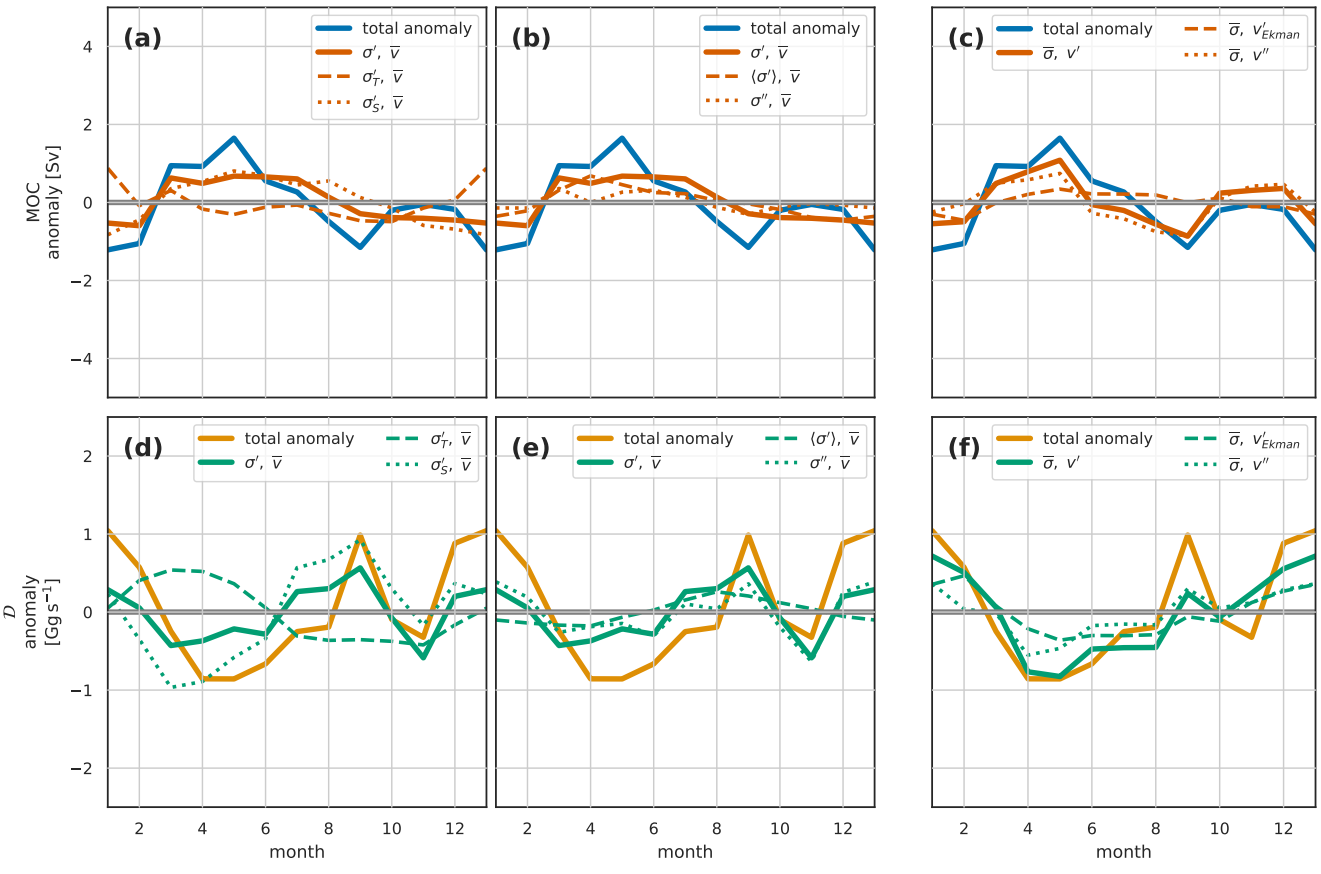

Figure 15. As for Fig 8 but for the **observed** seasonal cycle at **OSNAP$_W$**.

For freshwater transport (Figs. 16c,d and 17c,d) the seasonal cycle is also, to a large extent, driven by the barotropic velocity variability. With peak southward freshwater transport in winter and minimum in late summer in both observations and model. In contrast to the heat transport, the property variability term (here, salinity) is also plays a role (Figs. 16c and 17c) acting to shift the phase of the seasonal cycle of freshwater transport earlier in the year, with a spring minimum in southward freshwater transport and late summer/autumn maximum. This phase corresponds to the seasonal cycle of freshwater exiting southwards across the OSNAP line in the near-surface western boundary current. Notice that the salinity-driven variability lies entirely in our remainder term - rather than in the zonal-averaged salinity variability. This is because the largest seasonal salinity variability is confined to the southward flow at the western boundaries, rather than the broader zonal horizontal scale of surface temperature seasonal variability.

https://doi.org/10.5194/egusphere-2025-616
Preprint. Discussion started: 14 February 2025

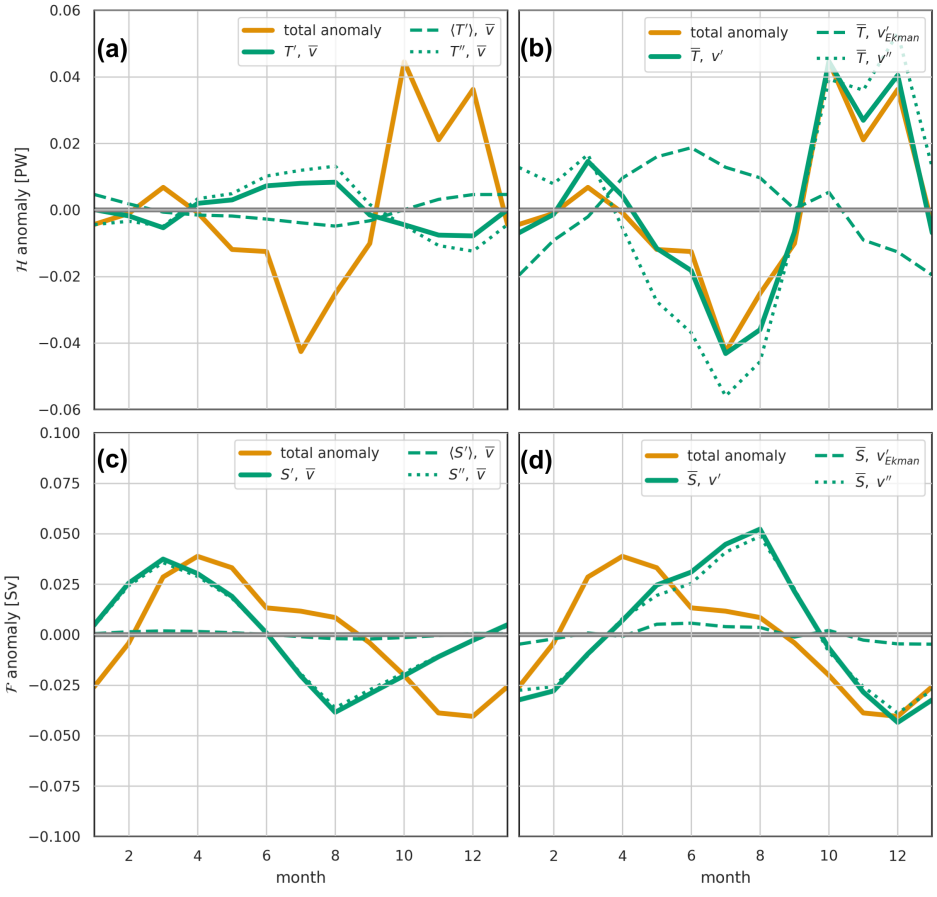

Figure 16. The **Modelled** OSNAP heat transport $\mathcal{H}$ (a,b) andfreshwater transport $\mathcal{F}$ (c,d) seasonal cycle. (a) Seasonal heat transport anomalies driven by temperature variability, mean velocities: solid yellow line – total anomaly; solid green – total temperature-driven anomaly; dashed line – component due to zonal mean temperature variability; component due to residual temperature variability. (b) Seasonal heat transport anomalies driven by velocity variability, mean temperatures: solid yellow line – total anomaly; solid green – total velocity-driven anomaly; dashed line – component due to Ekman transport variability; component due to residual velocity variability. (c) Seasonal freshwater transport anomalies driven by salinity variability, mean velocities: solid yellow line – total anomaly; solid green – total salinity-driven anomaly; dashed line – component due to zonal mean salinity variability; component due to residual salinity variability. (b) Seasonal freshwater transport anomalies driven by velocity variability, mean salinities: solid yellow line – total anomaly; solid green – total velocity-driven anomaly; dashed line – component due to Ekman transport variability; component due to residual velocity variability.

4 Discussion

We have examined the seasonal cycle of subpolar North Atlantic overturning in the overturning streamfunction and four associated metrics: the commonly used meridional overturning, MOC (the maximum of the streamfunction Ψ); heat transport and freshwater transport; and the less commonly considered density flux. We have looked at each of these in an eddy-resolving

https://doi.org/10.5194/egusphere-2025-616
Preprint. Discussion started: 14 February 2025

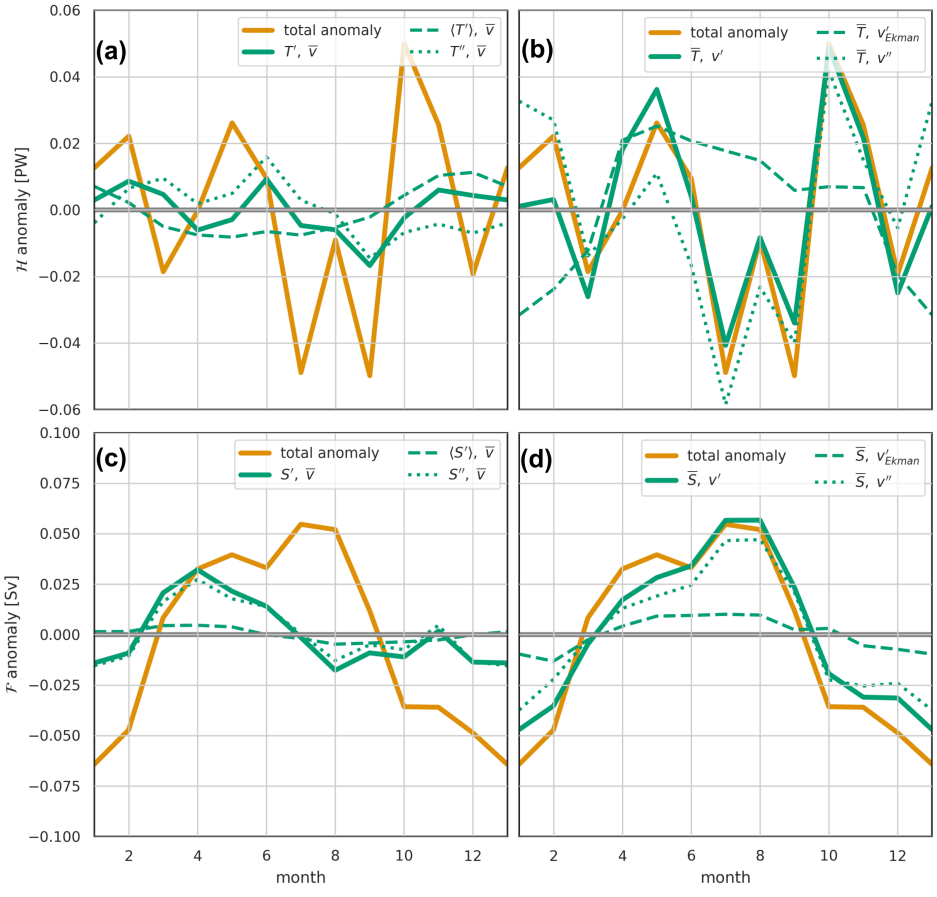

Figure 17. The **Observed** OSNAP heat transport $\mathcal{H}$ (a,b) and freshwater transport $\mathcal{F}$ (c,d) seasonal cycle. For a full description of the panels see Fig. 16.

model and in observational data from the OSNAP array. We have further divided these metrics into separate components driven by velocity and density variability. We have attempted to place these metrics in a coherent framework, particularly highlighting the relationship of the MOC and the density flux to the overturning streamfunction. The main results are summarised in Sect. 5, here we consider the following questions in a little more depth: Is the density-flux a useful (additional) metric for monitoring overturning? What may cause the differences between modelled and observed seasonal cycles? How do our results complement and advance previous studies of the seasonal cycles of subpolar overturning? What are the implications, if any, for the monitoring and study of lower frequency variability of the overturning circulation?

Firstly, the density flux. For the seasonal cycle each of the metrics considered is dominated by a different physical process or region. For example for the full OSNAP section seasonal cycle: MOC is mostly responding to a combination of the near-surface density in the western boundary current and Ekman transport variability; density flux is dominated by Ekman transport variability; heat flux by variability of non-Ekman, mostly barotropic, residual velocities; and freshwater flux responds to a

https://doi.org/10.5194/egusphere-2025-616
Preprint. Discussion started: 14 February 2025

combination of the barotropic velocities and the seasonal cycle of surface salinity in the western boundary. The density flux may not therefore appear very useful – mostly responding to the Ekman transport variability. However, this is largely due to the cancellation of density-driven seasonality in the density flux between $\mathrm{OSNAP_E}$ and $\mathrm{OSNAP_W}$,temperature variability dominating in $\mathrm{OSNAP_E}$ while salinity variability dominates in $\mathrm{OSNAP_W}$. As an integrated measure, rather than an extreme, density-flux is 'better' behaved than MOC: density fluxes sums, averages, trends and variability are simple to calculate; unlike MOC which needs to always be considered in the context of the σ_{MOC} value and, where possible analysis undertaken on the full streamfunction before calculating MOC. The MOC metric, at least for the seasonal cycle, is also extremely sensitive to variability in a very limited geographic region – for example variability in $\mathrm{OSNAP_E}$ is found to be entirely due to surface temperature variability in the Irminger basin and the East Greenland Current whereas density flux is sampling the whole basin including the North Atlantic Current. We might even conclude that the current focus of many overturning studies on the Irminger Basin and East Greenland Current is as much a function of the characteristics of the MOC metric as of the importance of these regions to overturning. Density flux turns out not to be a simple combination of heat and freshwater flux, this is highlighted here as both heat and freshwater flux seasonality are strongly influenced by the barotropic velocity variability, which plays only a minor part in the density flux seasonality. We suggest that density flux complements the more commonly used overturning metrics and as such would recommend that density flux becomes a routinely used additional metric, if not the primary metric, when studying the overturning circulation.

While modelled and observed seasonal cycles are largely consistent there are some differences. The observations show a larger Ekman-driven seasonal cycle, this is primarily due to the different averaging periods for the model and observations. When the model analysis is repeated on the observational time period the Ekman component is correspondingly stronger (Figs. S1-S3). The modelled seasonal cycles of both MOC and density flux show a larger contribution from the density-driven variability than the observations. Some of this is due to a weaker freshwater cycle in the model (the freshwater-driven overturning often opposes the heat-driven overturning), and some to a stronger seasonal cycle of near-surface temperature in the model, particularly in $\mathrm{OSNAP_E}$. This may be a function of the surface forcing dataset used in the Viking20x model, or alternatively an underestimate of the seasonal cycle of surface tenperature in the observations. We have shown how the MOC metric is extremely sensitive to temperature and salinity variability in quite confined regions of strong flow near the surface. Finally, and perhaps the largest difference between model and observational seasonal cycles, is the presence of high-frequency variability, particularly evident in the non-Ekman-driven velocity component in the observations. This is centred in $\mathrm{OSNAP_E}$ and in the barotropic velocities. Only a small part of this is due to the shorter period spanned by the observations (see Figs. S1-S3). This could be associated with missing model physics or the difficulty making high-quality observations of the barotropic currents with limited resources. The OSNAP gridding methodology, away from the boundary regions, assumes spatially-uniform barotropic velocities calculated as a volume-balance compensation velocity, these can involve rapidly-varying transports of tens of Sverdrups though we haven't been able to link this directly to the high-frequency variability observed here.

Observational and modelling studies of subpolar North Atlantic meridional overturning consistently return estimates of the seasonal cycle of overturning, as measured by the maximum of the overturning streamfunction (MOC_σ), with amplitude of

https://doi.org/10.5194/egusphere-2025-616
Preprint. Discussion started: 14 February 2025

about 4 Sv with a late spring maximum and autumn or winter minimum (Lozier et al., 2019; Fu et al., 2023; Wang et al., 2021; Tooth et al., 2023; Mercier et al., 2024). Our results, both model and observational confirm these general conclusions.

Published analyses, both model-based and observational, tend to focus on MOC seasonality, predominantly in the eastern subpolar gyre ($OSNAP_E$ and OVIDE). These show the subpolar AMOC seasonal cycle to be dominated by seasonality in the Irminger Basin, particularly the East Greenland Current, modified by Ekman transport driven by seasonality in the zonal winds (Wang et al., 2021; Fu et al., 2023; Tooth et al., 2023; Mercier et al., 2024). Observational (Le Bras et al., 2018; Mercier et al., 2024) and model (Tooth et al., 2023) analyses find the MOC variability due to the East Greenland Current to be a combination of density-field and transport variability - though it is difficult to disentangle the two due to the dominance of geostrophic currents. The results we obtain generally confirm the importance of Ekman and western boundary processes in the seasonality of MOC. However, we find little contribution from western boundary transports in either models or observations; the western boundary contribution to MOC being almost entirely explained by the zonal mean density variability. This is particularly notable because this zonal mean density variability has no associated zonal pressure gradients, so is uncoupled from the velocity fields.

The Irminger Basin and East Greenland Current density and transport seasonality have been ascribed to a lagged signal of watermass transformation and North Atlantic deep water (NADW) formation in the Irminger Basin (Fu et al., 2023), with the relatively short lag time attributed to the travel time from the transformation regions to $OSNAP_E$ (Le Bras et al., 2020; Fu et al., 2023). However Tooth et al. (2023) points out that the 4 Sv seasonal signal in overturning is much smaller than the 20 Sv seasonality in the watermass transformation in the Irminger Basin north of $OSNAP_E$, the difference between the two being seasonal heat storage and release from the surface waters. While we don't disagree with this lagged transformation diagnosis, we note that the seasonality of MOC is tied to the seasonality of the surface density structure, mostly summer/autumn warming and winter/spring cooling. This seasonality naturally lags the water transformation cycle which is tied to the surface fluxes, mostly due to the large heat capacity of seawater and vertical mixing. Given the basin-scale nature of the surface density cycle, and the similar large scale of seasonal surface heat fluxes (e.g. Berry and Kent, 2009) the simpler explanation of seasonal rise and fall of the σ_{MOC} isopycnal due to the local seasonal cycle of surface fluxes is perhaps more appropriate than that of advectively lagged water transformation. We note that advection certainly has a role in surface flux effects on density, but the estimated seasonal advective distances involved in even the fastest currents in the region (8 months around the northern segment of the Irminger Basin Tooth et al., 2023) are still relatively small compared to the length scales of seasonal surface fluxes.

We must emphasise that the location of the dominant $OSNAP_E$ overturning seasonality in the East Greenland Current is not new, it confirms the results of Wang et al. (2021); Fu et al. (2023); Tooth et al. (2023); Mercier et al. (2024). However we also emphasise that this local dominance is partly a feature of the MOC metric, since density, heat and freshwater flux seasonal cycles are less dominated by this single small region. The Irminger Basin and East Greenland Current dominance of the MOC seasonal cycle is due to a combination of two factors – the dominance of the cycle by near-surface seasonal density variability, and this region being the only part of $OSNAP_E$ where the σ_{MOC} isopycnal is within the depth range of this surface variability. MOC needs to be carefully interpreted in the context of σ_{MOC} position and variability.

https://doi.org/10.5194/egusphere-2025-616
Preprint. Discussion started: 14 February 2025

While these comparisons, and the exploration of mechanisms driving seasonality of the MOC overturning metric are enlightening, the more interesting result is how poorly the MOC metric seasonal cycle predicts the seasonal cycle in any of the integrated metrics – density, heat and freshwater fluxes – mostly due to its high sensitivity to a small set of processes in a limited geographical region. It is these integrated metrics, and how they evolve, which are arguably more relevant to understanding the potential changes to overturning seasonality which are most important for mitigating the impacts of AMOC changes on Atlantic sector weather and climate.

We now consider how our conclusions from analysis of the seasonal cycles may be extended to longer-term monitoring of the Atlantic meridional overturning circulation. The model-observation seasonal cycle differences require consideration from both large-scale overturning observational and modelling perspectives to improve confidence in observations and predictions of overturning. The largest differences found were in the representation of barotropic currents and near-surface seasonal temperature and salinity structures – particularly in the boundary currents – at depths which may be shallower than the upper sensors on longterm monitoring arrays. Both of these differences suggest possible focusses for improvement of long-term AMOC monitoring and climate modelling. Further, MOC is commonly used for climate model verification, however a focus on reproducing the MOC metric may be a poor guide to the quality of the modelled overturning circulation and property fluxes.

We find the most commonly considered MOC metric – the maximum of the overturning streamfunction – to be overly focussed on seawater property changes in a couple of small geographic regions: flows in the upper 500 m in the East Greenland Current and 1000 m in the Labrador Current. This is certainly the case on seasonal timescales, it may be a more reliable metric on longer timescales but this needs to be demonstrated. We also note that while $\mathrm{OSNAP_E}$ makes the largest contribution to all the metrics (except freshwater flux), focus on MOC perhaps exaggerates the comparative importance of $\mathrm{OSNAP_E}$ versus $\mathrm{OSNAP_W}$ to the overturning circulation and its wider implications; and within $\mathrm{OSNAP_E}$ MOC probably underemphasises the importance of the northward flows of warm and salty waters in the eastern subpolar gyre (Iceland Basin and Rockall Trough) to the overturning. We need to be mindful of all these characteristics of the MOC metric when designing observational campaigns. Heat and freshwater fluxes must also not be neglected as measures of overturning, our analysis finds these to be strongly influenced by the barotropic current variability. These barotropic currents are the currents which OSNAP (and RAPID) are most likely to get wrong, because the barotropic compensation transport is applied quite crudely. We suggest that this could specifically affect the accuracy of observed heat and freshwater flux estimates, while still appearing to get the right answer for MOC. In recent work Chafik and Lozier (2025) raise similar concerns about the use of the MOC metric, concluding that it essentially captures variability in upper ocean heat content, which can result from a number of mechanisms, some unrelated to overturning. There is a real danger that excessive, or exclusive focus on MOC could miss overturning 'slowdown' associated with unsampled variability, for example, with a changing density difference between upper and lower limbs rather than reduced net transport (Koman et al., 2024). The addition of use of the density flux metric would help capture such changes.

https://doi.org/10.5194/egusphere-2025-616
Preprint. Discussion started: 14 February 2025

5 Conclusions

We place meridional overturning and density, heat and freshwater fluxes in a coherent framework. This framework highlights the integral relationship between meridional overturning circulation and property transports, both being functions purely of the overturning streamfunction Ψ. Using this framework we examine the seasonality observed in overturning and density, temperature and freshwater fluxes at the OSNAP line in the subpolar North Atlantic. We find MOC seasonal cycles to be dominated by Ekman transports and large-scale seasonal cycle of surface density; heat flux seasonal cycles to be dominated by barotropic velocity variability; freshwater fluxes by a combination of barotropic velocities and the salinity in the western boundary current; and density fluxes to reflect a broad range of processes. We further show that the standard measure of overturning, the MOC metric, is a poor predictor, on seasonal time-scales, of either density fluxes or the more societally relevant ocean heat and freshwater transports. This is due to each of these metrics responding to different physical processes. The MOC metric in particular has very high sensitivity to near-surface physical processes in a limited geographical area. These processes are not necessarily reflective of the fundamental processes driving overturning. We find there to be a real danger that exclusive focus on MOC could miss overturning 'slowdown' associated unsampled variability, for example, with a changing density difference between upper and lower limbs rather than reduced net transport (Koman et al., 2024). The addition of use of the density flux metric would help capture such changes. Our results complement recent work of Chafik and Lozier (2025) raise similar concerns about the use of the MOC metric. We suggest caution in the use of the standard MOC metric in studies of overturning and the routine use of the density flux as a valuable additional metric.

Code/data availability

. ERA5 monthly averaged data on single levels from 1940 to present were obtained from Copernicus Climate Change Service (C3S) Climate Data Store (CDS) https://doi.org/10.24381/cds.f17050d7 (Hersbach et al., 2023) (Last accessed on 5-Oct-2024). Neither the European Commission nor ECMWF is responsible for any use that may be made of the Copernicus information or data it contains. The OSNAP data were downloaded from https://doi.org/10.35090/gatech/70342 (last accessed 3-Dec-2024). OSNAP data were collected and made freely available by the OSNAP (Overturning in the Subpolar North Atlantic Program) project and all the national programs that contribute to it () (Fu et al., 2023). The full output for the simulation VIKING20X-JRA-short is available at https://doi.org/10.26050/WDCC/VIKING20XJRAshort (Getzlaff and Schwarzkopf, 2024). The subset of VIKING20X-JRA-short output used in this study can be obtained on request from the authors and will be made publicly available before final publication. The code to perform the analysis described was written in Jupyter notebooks in Python and again can be obtained on request from the authors and will be made publicly available before final publication.

https://doi.org/10.5194/egusphere-2025-616
Preprint. Discussion started: 14 February 2025

Author contribution

. ADF defined the overall research problem, the methodology and performed the analyses. All co-authors discussed and refined the analyses and contributed to the text.

6 Competing interests

. There are no competing interests

Acknowledgements

. This work was supported by the UK Natural Environment Research Council (NERC) grants UK-OSNAP (NE/K010875/2), UK-OSNAP-Decade (NE/T00858X/1), and SNAP-DRAGON (NE/T013494/1), and by the NERC National Capability programme CLASS (NE/R015953/1). The ocean model simulation VIKING20X-JRA-short was performed at the North German Supercomputing Alliance (HLRN).

https://doi.org/10.5194/egusphere-2025-616
Preprint. Discussion started: 14 February 2025

References

Berry, D. I. and Kent, E. C.: A New Air–Sea Interaction Gridded Dataset from ICOADS With Uncertainty Estimates, Bulletin of the American Meteorological Society, 90, 645–656, https://doi.org/10.1175/2008BAMS2639.1, 2009.

Biastoch, A., Schwarzkopf, F. U., Getzlaff, K., Rühs, S., Martin, T., Scheinert, M., Schulzki, T., Handmann, P., Hummels, R., and Böning, C. W.: Regional imprints of changes in the Atlantic Meridional Overturning Circulation in the eddy-rich ocean model VIKING20X, Ocean Science, 17, 1177–1211, https://doi.org/10.5194/os-17-1177-2021, 2021.

Chafik, L. and Lozier, M. S.: When Simplification Leads to Ambiguity: A Look at Two Ocean Metrics for the Subpolar North Atlantic, Geophysical Research Letters, 52, e2024GL112 496, https://doi.org/10.1029/2024GL112496, 2025.

Chidichimo, M. P., Kanzow, T., Cunningham, S. A., Johns, W. E., and Marotzke, J.: The contribution of eastern-boundary density variations to the Atlantic meridional overturning circulation at 26.5° N, Ocean Science, 6, 475–490, https://doi.org/10.5194/OS-6-475-2010, 2010.

Cunningham, S. A., Kanzow, T., Rayner, D., Baringer, M. O., Johns, W. E., Marotzke, J., Longworth, H. R., Grant, E. M., Hirschi, J. J., Beal, L. M., Meinen, C. S., and Bryden, H. L.: Temporal variability of the Atlantic meridional overturning circulation at 26.5°N, Science, 317, 935–938, https://doi.org/10.1126/SCIENCE.1141304/SUPPL_FILE/CUNNINGHAM.SOM.PDF, 2007.

Forget, G., Campin, J. M., Heimbach, P., Hill, C. N., Ponte, R. M., and Wunsch, C.: ECCO version 4: An integrated framework for non-linear inverse modeling and global ocean state estimation, Geoscientific Model Development, 8, https://doi.org/10.5194/gmd-8-3071-2015, 2015.

Fraser, N. J. and Cunningham, S. A.: 120 Years of AMOC Variability Reconstructed From Observations Using the Bernoulli Inverse, Geophysical Research Letters, 48, e2021GL093 893, https://doi.org/10.1029/2021GL093893, 2021.

Fraser, N. J., Fox, A. D., Cunningham, S. A., Rath, W., Schwarzkopf, F. U., and Biastoch, A.: Vertical Velocity Dynamics in the North Atlantic and Implications for AMOC, Journal of Physical Oceanography, 54, 2011–2024, https://doi.org/10.1175/JPO-D-23-0229.1, 2024.

Fraser, N. J., Fox, A. D., and Cunningham, S. A.: Impact of Ekman Pumping on the Meridional Coherence of the AMOC, Geophysical Research Letters, 52, e2024GL108 846, https://doi.org/10.1029/2024GL108846, 2025.

Fu, Y., Lozier, M. S., Biló, T. C., Bower, A. S., Cunningham, S. A., Cyr, F., de Jong, M. F., deYoung, B., Drysdale, L., Fraser, N., Fried, N., Furey, H. H., Han, G., Handmann, P., Holliday, N. P., Holte, J., Inall, M. E., Johns, W. E., Jones, S., Karstensen, J., Li, F., Pacini, A., Pickart, R. S., Rayner, D., Straneo, F., and Yashayaev, I.: Seasonality of the Meridional Overturning Circulation in the subpolar North Atlantic, Communications Earth and Environment 2023 4:1, 4, 1–13, https://doi.org/10.1038/s43247-023-00848-9, 2023.

Gary, S. F., Cunningham, S. A., Johnson, C., Houpert, L., Holliday, N. P., Behrens, E., Biastoch, A., and Böning, C. W.: Seasonal cycles of oceanic transports in the eastern subpolar North Atlantic, Journal of Geophysical Research: Oceans, 123, 1471–1484, https://doi.org/10.1002/2017JC013350, 2018.

Getzlaff, K. and Schwarzkopf, F. U.: VIKING20X-JRA-short: daily to multi-decadal ocean dynamics under JRA55-do atmospheric forcing., World Data Center for Climate (WDCC) at DKRZ, https://doi.org/10.26050/WDCC/VIKING20XJRAshort, [Dataset], 2024.

Han, L.: Mechanism on the Short-Term Variability of the Atlantic Meridional Overturning Circulation in the Subtropical and Tropical Regions, Journal of Physical Oceanography, 53, 2231–2244, https://doi.org/10.1175/JPO-D-23-0027.1, 2023a.

Han, L.: Exploring the AMOC Connectivity Between the RAPID and OSNAP Lines With a Model-Based Data Set, Geophysical Research Letters, 50, e2023GL105 225, https://doi.org/10.1029/2023GL105225, 2023b.

Hersbach, H., Bell, B., Berrisford, P., Hirahara, S., Horányi, A., Muñoz-Sabater, J., Nicolas, J., Peubey, C., Radu, R., Schepers, D., Simmons, A., Soci, C., Abdalla, S., Abellan, X., Balsamo, G., Bechtold, P., Biavati, G., Bidlot, J., Bonavita, M., Chiara, G. D.,

https://doi.org/10.5194/egusphere-2025-616
Preprint. Discussion started: 14 February 2025

Dahlgren, P., Dee, D., Diamantakis, M., Dragani, R., Flemming, J., Forbes, R., Fuentes, M., Geer, A., Haimberger, L., Healy, S., Hogan, R. J., Hólm, E., Janisková, M., Keeley, S., Laloyaux, P., Lopez, P., Lupu, C., Radnoti, G., de Rosnay, P., Rozum, I., Vamborg, F., Villaume, S., and Thépaut, J.-N.: The ERA5 global reanalysis, Quarterly Journal of the Royal Meteorological Society, 146, 1999–2049, https://doi.org/10.1002/QJ.3803, 2020.

Hersbach, H., Bell, B., Berrisford, P., Biavati, G., Horányi, A., Muñoz-Sabater, J., Nicolas, J., Peubey, C., Radu, R., Rozum, I., Schepers, D., Simmons, A., Soci, C., Dee, D., and Thépaut, J.-N.: ERA5 monthly averaged data on single levels from 1940 to present, Copernicus Climate Change Service (C3S) Climate Data Store (CDS), https://doi.org/10.24381/cds.f17050d7, [Dataset] (Accessed on 5-Oct-2024), 2023.

Hirschi, J. J., Barnier, B., Böning, C., Biastoch, A., Blaker, A. T., Coward, A., Danilov, S., Drijfhout, S., Getzlaff, K., Griffies, S. M., Hasumi, H., Hewitt, H., Iovino, D., Kawasaki, T., Kiss, A. E., Koldunov, N., Marzocchi, A., Mecking, J. V., Moat, B., Molines, J. M., Myers, P. G., Penduff, T., Roberts, M., Treguier, A. M., Sein, D. V., Sidorenko, D., Small, J., Spence, P., Thompson, L. A., Weijer, W., and Xu, X.: The Atlantic Meridional Overturning Circulation in High-Resolution Models, Journal of Geophysical Research: Oceans, 125, https://doi.org/10.1029/2019JC015522, 2020.

Johnson, H. L., Cessi, P., Marshall, D. P., Schloesser, F., and Spall, M. A.: Recent Contributions of Theory to Our Understanding of the Atlantic Meridional Overturning Circulation, Journal of Geophysical Research: Oceans, 124, 5376–5399, https://doi.org/10.1029/2019JC015330, 2019.

Kanzow, T., Cunningham, S. A., Rayner, D., Hirschi, J. J., Johns, W. E., Baringer, M. O., Bryden, H. L., Beal, L. M., Meinen, C. S., and Marotzke, J.: Observed flow compensation associated with the MOC at 26.5°N in the Atlantic, Science, 317, 938–941, https://doi.org/10.1126/SCIENCE.1141293/SUPPL_FILE/KANZOW-SOM.PDF, 2007.

Koman, G., Bower, A. S., Holliday, N. P., Furey, H. H., Fu, Y., and Biló, T. C.: Observed decrease in Deep Western Boundary Current transport in subpolar North Atlantic, Nature Geoscience 2024 17:11, 17, 1148–1153, https://doi.org/10.1038/s41561-024-01555-6, 2024.

Le Bras, I. A.-A., Straneo, F., Holte, J., and Holliday, N. P.: Seasonality of Freshwater in the East Greenland Current System From 2014 to 2016, Journal of Geophysical Research: Oceans, 123, 8828–8848, https://doi.org/10.1029/2018JC014511, 2018.

Le Bras, I. A.-A., Straneo, F., Holte, J., de Jong, M. F., and Holliday, N. P.: Rapid Export of Waters Formed by Convection Near the Irminger Sea's Western Boundary, Geophysical Research Letters, 47, e2019GL085 989, https://doi.org/10.1029/2019GL085989, 2020.

Lozier, M. S., Li, F., Bacon, S., Bahr, F., Bower, A. S., Cunningham, S. A., de Jong, M. F., de Steur, L., DeYoung, B., Fischer, J., Gary, S. F., Greenan, B. J. W., Holliday, N. P., Houk, A., Houpert, L., Inall, M. E., Johns, W. E., Johnson, H. L., Johnson, C., Karstensen, J., Koman, G., Le Bras, I. A., Lin, X., Mackay, N., Marshall, D. P., Mercier, H., Oltmanns, M., Pickart, R. S., Ramsey, A. L., Rayner, D., Straneo, F., Thierry, V., Torres, D. J., Williams, R. G., Wilson, C., Yang, J., Yashayaev, I., and Zhao, J.: A sea change in our view of overturning in the subpolar North Atlantic, Science, 363, 516+, https://doi.org/10.1126/science.aau6592, 2019.

Mercier, H., Desbruyères, D., Lherminier, P., Velo, A., Carracedo, L., Fontela, M., and Pérez, F. F.: New insights into the eastern subpolar North Atlantic meridional overturning circulation from OVIDE, Ocean Science, 20, 779–797, https://doi.org/10.5194/OS-20-779-2024, 2024.

Nurser, A. J., Marsh, R., and Williams, R. G.: Diagnosing water mass formation from air-sea fluxes and surface mixing, Journal of Physical Oceanography, 29, 1468–1487, https://doi.org/10.1175/1520-0485(1999)029<1468:DWMFFA>2.0.CO;2, 1999.

Petit, T., Lozier, M. S., Josey, S. A., and Cunningham, S. A.: Atlantic Deep Water Formation Occurs Primarily in the Iceland Basin and Irminger Sea by Local Buoyancy Forcing, Geophysical Research Letters, 47, e2020GL091 028, https://doi.org/10.1029/2020GL091028, 2020.

https://doi.org/10.5194/egusphere-2025-616
Preprint. Discussion started: 14 February 2025

Speer, K. and Tziperman, E.: Rates of Water Mass Formation in the North Atlantic Ocean, Journal of Physical Oceanography, 22, 93–104, https://doi.org/10.1175/1520-0485(1992)022<0093:rowmfi>2.0.co;2, 1992.

Tooth, O. J., Johnson, H. L., Wilson, C., and Evans, D. G.: Seasonal overturning variability in the eastern North Atlantic subpolar gyre: a Lagrangian perspective, Ocean Science, 19, 769–791, https://doi.org/10.5194/OS-19-769-2023, 2023.

Tziperman, E.: On the role of interior mixing and air-sea fluxes in determining the stratification and circulation of the oceans, Journal of Physical Oceanography, 16, 680–693, https://doi.org/10.1175/1520-0485(1986)016<0680:OTROIM>2.0.CO;2, 1986.

Wang, H., Zhao, J., Li, F., and Lin, X.: Seasonal and Interannual Variability of the Meridional Overturning Circulation in the Subpolar North Atlantic Diagnosed From a High Resolution Reanalysis Data Set, Journal of Geophysical Research: Oceans, 126, https://doi.org/10.1029/2020JC017130, 2021.

Yang, J.: Local and remote wind stress forcing of the seasonal variability of the Atlantic Meridional Overturning Circulation (AMOC) transport at 26.5N, Journal of Geophysical Research: Oceans, 120, https://doi.org/10.1002/2014JC010317, 2015.

Zhao, J. and Johns, W.: Wind-driven seasonal cycle of the atlantic meridional overturning circulation, Journal of Physical Oceanography, 44, https://doi.org/10.1175/JPO-D-13-0144.1, 2014.